

# Fused and vaulted nasals of tyrannosaurid dinosaurs: Implications for cranial strength and feeding mechanics

ERIC SNIVELY, DONALD M. HENDERSON, and DOUG S. PHILLIPS



Snively, E., Henderson, D.M., and Phillips, D.S. 2006. Fused and vaulted nasals of tyrannosaurid dinosaurs: Implications for cranial strength and feeding mechanics. *Acta Palaeontologica Polonica* 51 (3): 435–454.

Tyrannosaurid theropods display several unusual adaptations of the skulls and teeth. Their nasals are fused and vaulted, suggesting that these elements braced the cranium against high feeding forces. Exceptionally high strengths of maxillary teeth in *Tyrannosaurus rex* indicate that it could exert relatively greater feeding forces than other tyrannosaurids. Areas and second moments of area of the nasals, calculated from CT cross-sections, show higher nasal strengths for large tyrannosaurids than for *Allosaurus fragilis*. Cross-sectional geometry of theropod crania reveals high second moments of area in tyrannosaurids, with resulting high strengths in bending and torsion, when compared with the crania of similarly sized theropods. In tyrannosaurids trends of strength increase are positively allometric and have similar allometric exponents, indicating correlated progression towards unusually high strengths of the feeding apparatus. Fused, arched nasals and broad crania of tyrannosaurids are consistent with deep bites that impacted bone and powerful lateral movements of the head for dismembering prey.

**Key words:** Theropoda, Carnosauria, Tyrannosauridae, biomechanics, feeding mechanics, computer modeling, computed tomography.

Eric Snively [esnively@ucalgary.ca], Department of Biological Sciences, University of Calgary, 2500 University Drive NW, Calgary, Alberta T2N 1N4, Canada;

Donald M. Henderson [don.henderson@gov.ab.ca], Royal Tyrrell Museum of Palaeontology, Box 7500, Drumheller, Alberta T0J 0Y0, Canada;

Doug S. Phillips [phillips@ucalgary.ca], Department of Information Technologies, University of Calgary, 2500 University Drive NW, Calgary, Alberta T2N 1N4, Canada.

## Introduction

Large theropod dinosaurs display remarkable specializations for macrocarnivory (Holtz 2002), but tyrannosaurids take many of these feeding adaptations to an extreme. The Tyrannosauridae were giant coelurosaurian theropods from the Cretaceous of Asia and North America (Holtz 1994, 2004). Tyrannosaurids differ from both smaller coelurosaurs and other large theropods including carnosaurs (Fig. 1; Hutchinson and Padian 1997) in the greater robustness of their teeth (Farlow et al. 1991) and skulls (Henderson 2002; Therrien et al. 2005), enlarged areas for attachment and expansion of jaw muscles (Molnar 1973, 2000), and the consequent ability to bite deeply into bone (Abler 1992; Carpenter 2000; Chin 1998; Erickson et al. 1996; Meers 2003). Among other specific adaptations suggested for this activity, adult tyrannosaurid mandibles were stronger than those of other large theropods (Fig. 2). Large tyrannosaurid dentaries have high section moduli and could withstand high feeding forces two to four times higher than in equivalently sized carnosaurs (Therrien et al. 2005; Fig. 2, Appendix 1), and also have posteriorly declined and sometimes interdigitating mandibular symphyses that braced against shear and torsion (Therrien et al. 2005).

Tyrannosaurids and their closest relatives within the Tyrannosauroidae (Holtz 2004) are also distinguished from other theropods in the morphology of their nasals (Fig. 1). These elements are fused together in nearly all tyrannosaurid specimens and invariably display arch-like vaulting [Brochu 2003; Currie 2003a; Hutt et al. 2001; Xu et al. 2004; only one apparently unfused specimen is known (Chris Morrow, personal communication 2004) out of dozens collected]. Fusion and vaulting are present in tyrannosauroid nasal specimens regardless of size, and throughout the history of the group (165–65 Ma; Xu et al. 2006b; Currie 2003a). The vaulted nasals form the top of a broad transverse arch of bone including the maxillae, in contrast to the narrow muzzles of most other theropods (Molnar and Farlow 1990; Meers 2003).

## Hypotheses and approach

The fusion and vaulting of tyrannosaurid nasals, and their position as the keystone (Busbey 1995) of a broad, strongly articulated nasal-maxillary arch, suggest that the nasals enhanced the strength of the snout against compressive, bending, shear, and torsional forces. The confluence of unusual mandible, tooth, and nasal morphologies in the Tyranno-

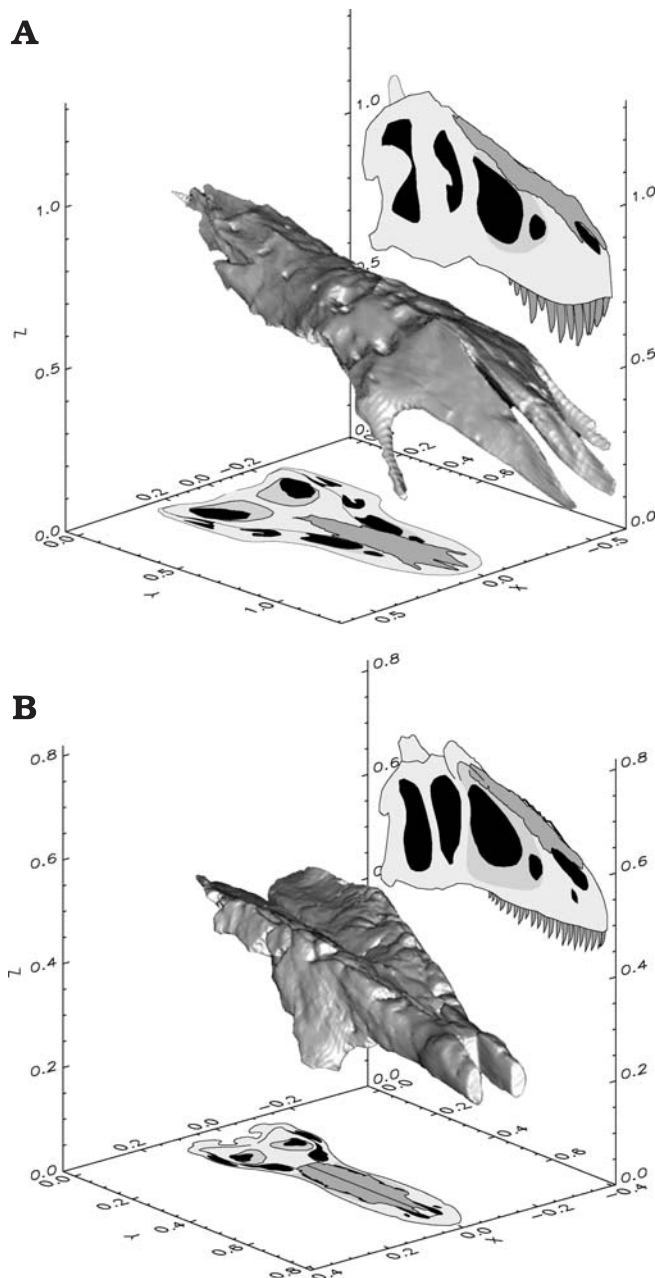


Fig. 1. Comparison of cranial and nasal morphology of: **A**, the tyrannosaurid *Tyrannosaurus rex* (TMP 98.86.01; cast of BHI 2033) and **B**, the carnosaur *Allosaurus fragilis* (UUVP 1663/UMNH VP 9146; mirrored to depict a complete pair). Scale axes for crania are in meters. Nasals in their life positions are highlighted in lateral and dorsal cranial views, and rendered in oblique view (not to scale). The *T. rex* nasals are tall, vaulted, and fused, while the *A. fragilis* nasals are lower and unfused.

sauridae suggests a correlated progression (Thomson 1966; Kemp 1999) towards a reinforced head skeleton and high bite power.

Using data derived from CT cross-sections of theropod nasals, analysis of cross-sectional geometry of theropod crania, and measurements of maxillary teeth, we tested several hypotheses related to possible correlated progression of the tyrannosaurid feeding apparatus:

(1) Tyrannosaurid maxillary teeth were stronger in bending those of other large carnivorous dinosaurs.

(2) Vaulting contributed significantly to tyrannosaurid nasal strength.

(3) Fusion of tyrannosaurid nasals imparted higher torsional and shear strengths than those of *Allosaurus* nasals.

(4) Tyrannosaurid crania were stronger in bending and torsion than carnosaur crania of similar length.

We approach these hypotheses inductively, proceeding from tooth to nasal to cranial strengths. The teeth were the elements that would first encounter resistance of prey tissues and would transmit food reaction forces to the cranium. Tyrannosaurid nasals were potentially adapted to resisting those forces, as dorsally positioned compressive members of the truss-like cranium (Molnar 2000; Rayfield 2004). We chose this order of investigation because each inductive stage can potentially falsify our overall hypothesis of correlated progression, and will build up to an integrated picture of the strengths of theropod feeding apparatus.

To compare these strengths, we used simple engineering principles and calculations. Simplified models of biological structures have a rich history in the palaeontological and neontological literature (Alexander 1985; Farlow et al. 1995; Greaves 1978, 1991; Henderson 2002; Holtz 1995; Molnar 2000; Slijper 1946; Thomason and Russell 1986; Thompson 1917). Simple approximations are valuable for numerous reasons, especially in palaeontology.

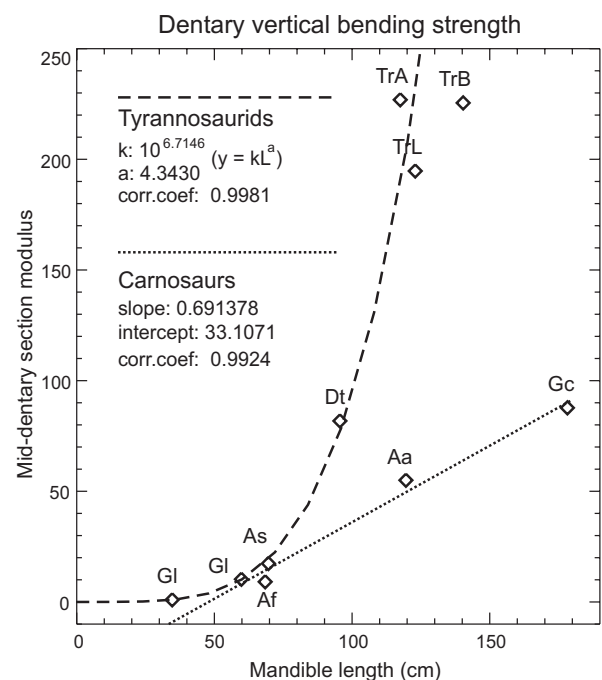


Fig. 2. Comparison of vertical bending strengths of adult theropod dentaries, graphed as mid-dentary section modulus versus mandible length (data from Therrien et al. 2005). Lines fitted by least squares regression, by log transformed values for the tyrannosaurid data. Carnosaur dentary strengths scale linearly with dentary length, while tyrannosaurid dentary strengths show an exponential increase. The tyrannosaurid dentaries are stronger than those of carnosaur for a given mandible length, indicating a relatively stronger bite. See Appendix 1 for specimen labels; Gc, *Giganotosaurus carolinii*.

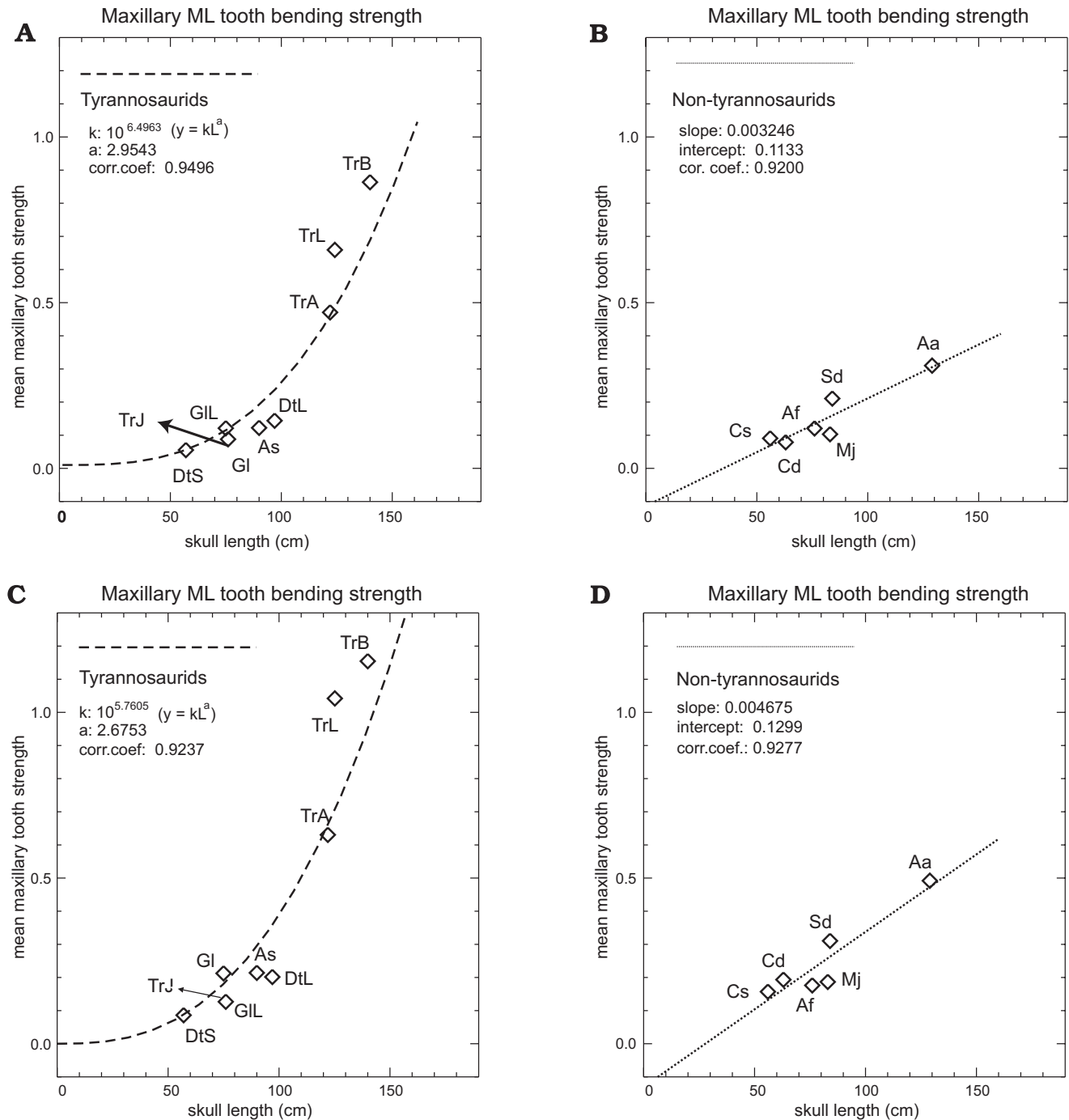


Fig. 3. Comparisons of mediolateral (A, B) and anteroposterior (C, D) strengths of tyrannosaurid and non-tyrannosaurid theropod maxillary teeth, plotted against skull length. Regressions are by least squares, on log transformed data for the tyrannosaurids. Trend lines are allometric in the tyrannosaurids but linear in non-tyrannosaurids. Tooth strengths of *Tyrannosaurus rex* are much higher than in any other examined taxon. Starting points of the small arrows indicate the position of the juvenile *T. rex* (TrJ). See Appendix 1 for other specimen labels.

First, reductionist models allow efficient tests of strength hypotheses by equations of beam theory and its elaborations (Young and Budynas 2001). These methods are applicable to cantilevered structures regardless of the proportions or shape of the beam (Molnar 2000; Henderson 2002) or truss (Rayfield 2004). Second, simple computational models can be constructed quickly, enabling assessment of variation across taxa. In contrast, 3D finite element modeling is time consum-

ing and usually encompasses one taxon at a time (Rayfield et al. 2001; Snively and Russell 2002; Mazzetta et al. 2004; Rayfield 2005). Third, simple analyses, as of skull and metatarsal function (Bakker 2000; Holtz 1994; Molnar 1973, 2000; Snively and Russell 2003; Snively et al. 2004), yield rapid generation of results and hypotheses that are testable by more sophisticated means (Rayfield et al. 2001; Rayfield 2004; Snively and Russell 2002). Conversely, elaborate tests

(Rayfield et al. 2001) are subject to refinement of assumptions, whose effects are more easily testable with simplified methods (Rayfield 2004).

Using shell-like theropod cranial models to test relative strengths exemplifies this approach. Models incorporating the influence of intracranial joints, cranial fenestration, and the palate (Rayfield 2005) will be valuable for future studies, because these factors affected second moments of area and hence bending and torsional strengths. We did not construct them here for several reasons. Fenestration occurred in areas where stresses would otherwise be minimal (Molnar 2000; Rayfield et al. 2001), stress concentrations will be similar overall in shell-like and lattice models (Gordon 1978; Greaves 1985), and a shell-like model does not obscure relative strengths of theropod crania.

For our purposes, the main benefit of the shell-like models is that they isolate the effects of geometry from other factors contributing to cranial strength. Tyrannosaurid crania had proportionally more bone and smaller fenestrae than did carnosaurs (Henderson 2002), and larger and presumably stronger ligamentous joints for resisting tension along the ventral border of the cranium (Rayfield 2004). The anterior secondary palate of tyrannosaurids (Holtz 2002) would greatly increase the torsional strength of the tyrannosaurid rostrum over that in some carnosaurs (contact of the palatal shelves in synapsids increased torsional strength immensely: Thomason and Russell 1986; Busby 1995). We gave the more open carnosaur specimens a relative advantage by approximating all crania as equally "closed" structures, effectively putting tyrannosaurid cranial geometry to a more stringent test.

*Institutional abbreviations.*—AMNH, American Museum of Natural History, New York, New York, USA; BHI, Black Hills Institute of Geological Research, Hill City, South Dakota, USA; BMRP, Burpee Museum of Natural History, Rockford, Illinois, USA; FMNH, Field Museum of Natural History, Chicago, Illinois, USA; IVPP, Institute of Vertebrate Palaeontology and Palaeoanthropology, Beijing, China; LACM, Natural History Museum of Los Angeles County, Los Angeles, California, USA; ROM, Royal Ontario Museum, Toronto, Ontario, Canada; MACN, Museo Argentino de Ciencias Naturales, Buenos Aires, Argentina; MOR, Museum of the Rockies, Bozeman, Montana, USA; MWC, Museum of Western Colorado, Grand Junction, Colorado, USA; NCSM, North Carolina State Museum of Natural Sciences, Raleigh, North Carolina, USA; SGM, Ministère de l'Énergie et des Mines, Rabat, Morocco; TCMI, The Children's Museum of Indianapolis, Indianapolis, Indiana, USA; TMP, Royal Tyrrell Museum of Palaeontology, Drumheller, Alberta, Canada; UUVP, University of Utah Vertebrate Paleontology, Salt Lake City, Utah, USA.

## Strengths of large theropod teeth

**Materials and methods for testing tooth strength of large theropods.**—We measured *in situ* maxillary teeth of large theropods (Table 1, Appendix 1) to determine if the tyrannosaurid teeth were stronger than those of non-tyrannosaurids, and to reveal any trends in tooth strength with increases in body size. Specimens included tyrannosaurids, carnosaurs,

Table 1. Measured and computed properties of theropod maxillary teeth. N, number of teeth measured; CH, average crown height; FABL, average fore, aft basal length; MLBL, average mediolateral basal length; AP str., average anteroposterior bending strength indicator; ML str., mediolateral bending strength indicator; Skull l., skull length. Raw measurements of CH, FABL, and MLBL, not these averages, were used to calculate strength indicators.

	N	CH (mm)	FABL (mm)	MLBL (mm)	AP str. m <sup>3</sup>	ML str. m <sup>3</sup>	Skull l. cm
Tyrannosauridae							
<i>Albertosaurus sarcophagus</i> (As)	7	70	29.9	17	0.214	0.122	86.0
<i>Daspletosaurus torosus</i> (DtS)	9	37.9	16.8	11.1	0.086	0.055	57.3
<i>Daspletosaurus torosus</i> (DtL)	6	72.5	27.3	19.7	0.202	0.144	97.0
<i>Gorgosaurus libratus</i> (Gl)	13	54.8	22.90	12.90	0.12	0.213	75.0
<i>Gorgosaurus libratus</i> (GIL)	11	57.1	23.13	22.6	0.127	0.088	76.0
<i>Tyrannosaurus rex</i> (TrA)	10	101.6	37.0	28.20	0.471	0.630	119.0
<i>Tyrannosaurus rex</i> (TrB)	11	98.4	45.0	33.50	0.864	1.154	140.0
<i>Tyrannosaurus rex</i> (TrL)	9	78.6	41.4	25.70	0.659	1.042	122.0
<i>Tyrannosaurus rex</i> juv. (TrJ)	11	45.5	22.6	11.20	0.131	0.065	74.0
Non-tyrannosaurids							
<i>Acrocanthosaurus atokensis</i> (Aa)	1	84.0	31.0	19.5	0.492	0.310	105.0
<i>Allosaurus fragilis</i> (Af)	14	44.3	18.40	12.70	0.121	0.176	76.0
<i>Carnotaurus sastrei</i> (Cs)	12	47.5	22.60	15.70	0.211	0.310	56.0
<i>Ceratopsaurus dentisulcatus</i> (Cd)	10	62.9	26.10	10.60	0.079	0.193	63.0
<i>Monolophosaurus jiangi</i> (Mj)	13	39.8	19.80	11.00	0.103	0.187	83.0
<i>Sinraptor dongi</i> (Sd)	12	47.5	22.60	15.70	0.211	0.310	84.0

and neoceratosaurians. Maxillary tooth measurements of the carnosaur *Acrocanthosaurus atokensis* were obtained from the literature (Harris 1998; Currie and Carpenter 2000).

Measurements (with Mitutoyo 505–634 calipers) were crown height, fore-aft basal length (FABL) and mediolateral basal length (MLBL), *sensu* Farlow et al. (1991). Because teeth of *Tyrannosaurus rex* BHI 2033 had taphonomically slipped out of the alveoli, their cross sectional measurements were taken from the proximal base of the enamel, and crown heights measured from this point as well. Strength indicators for maxillary teeth in mediolateral and anteroposterior bending were determined by calculating their section modulus after Farlow et al. (1991; assuming a rectangular cross-section), dividing by crown height, and assuming a unit force.

These tooth strength indicators were plotted against skull length. Skull lengths (from the anterior tip of the premaxilla to the posterior edge of the quadrates in lateral view) were measured with a tape measure, taken from the literature, or calculated from maxillary measurements and the log form of regression equations in Currie (2003b). The predicted lengths of measured skulls were within 3% of their actual lengths. However, for disarticulated skulls whose lengths were calculated using the regression equations (TCMI 2001.89.01; TMP 1994.143.1, 2001.36.1, and 2004.03.03), future published lengths from reconstructed skulls will be more definitive than those calculated here.

#### Results for maxillary tooth bending strengths.—

Table 1 enumerates average measurements and strength results for theropod maxillary teeth, and Fig. 3 plots mean maxillary tooth strengths versus theropod skull lengths. Fitted trend lines (using least squares regression) are shown for tyrannosaurids and carnosaurids, with the neoceratosaurians plotted as well. Smaller tyrannosaurid teeth are generally weaker in anteroposterior and mediolateral bending than teeth of non-tyrannosaurids. Maxillary teeth of most large tyrannosaurids are as strong or slightly stronger in mediolateral bending and stronger in anteroposterior bending than teeth of non-tyrannosaurids, except for the large carnosaur *Sinraptor dongi* and *Acrocanthosaurus atokensis*. *Tyrannosaurus rex* has much higher tooth strengths than these carnosaurids or other large tyrannosaurids. The average strengths of *T. rex* teeth are extraordinarily high relative to skull length, despite marked discrepancies in tooth sizes along each specimen's maxillary row (evident in the lower average strength in AMNH 5027). The patterns of increasing tooth strength with skull length differ between tyrannosaurids and other large theropods. The line of best fit for the non-tyrannosaurids is linear, while that for the tyrannosaurids is best described by an exponential function.

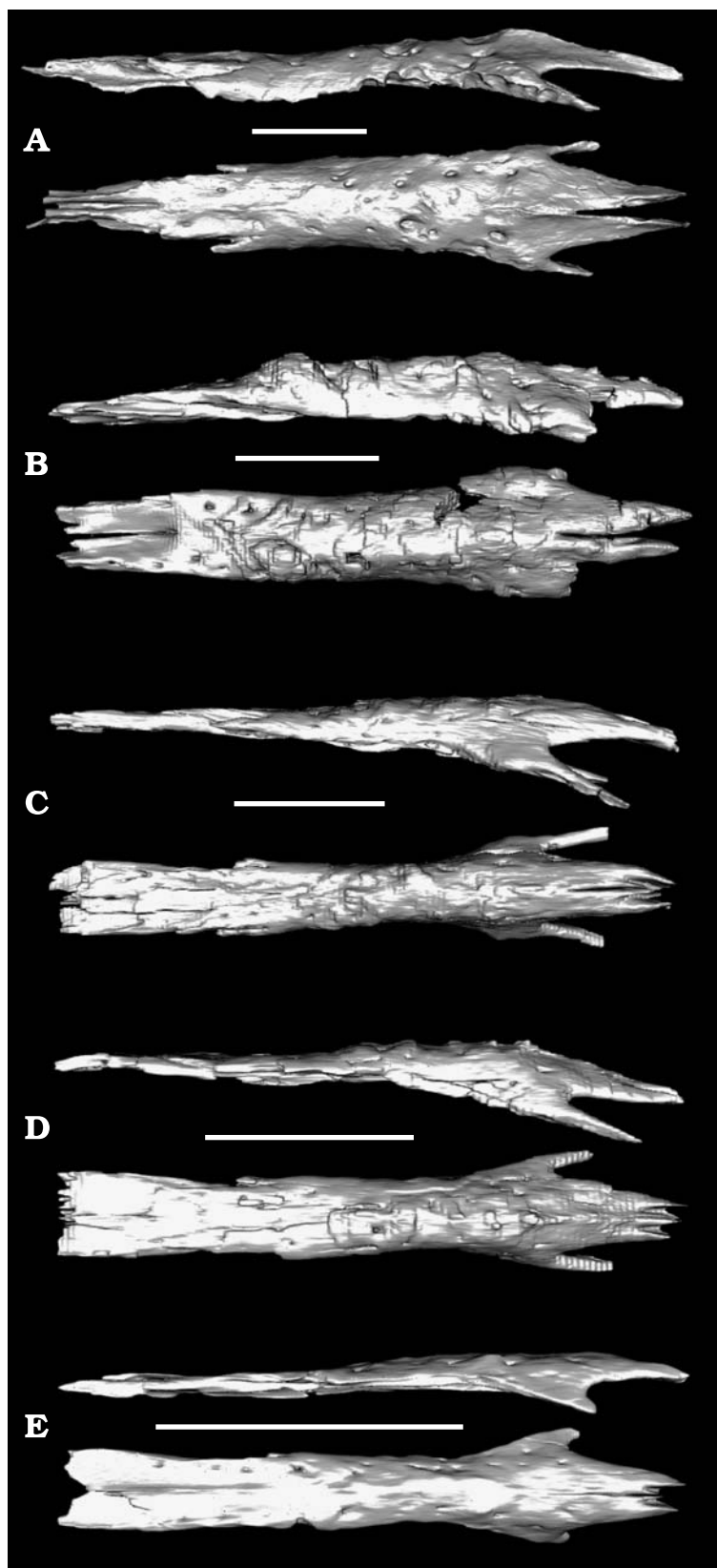


Fig. 4. CT reconstructions of tyrannosaurid nasals in side and top views. Anterior is to the right. A. *Tyrannosaurus rex* (TMP 98.86.01; cast of BHI 2033). B. *Daspletosaurus torosus* (TMP 98.48.1). C. *Albertosaurus sarcophagus* (TMP 2000.12.1). D. Adult *Gorgosaurus libratus* (TMP 86.64.1). E. Juvenile *Gorgosaurus libratus* (TMP 86.144.1). Scale bars 15 cm.

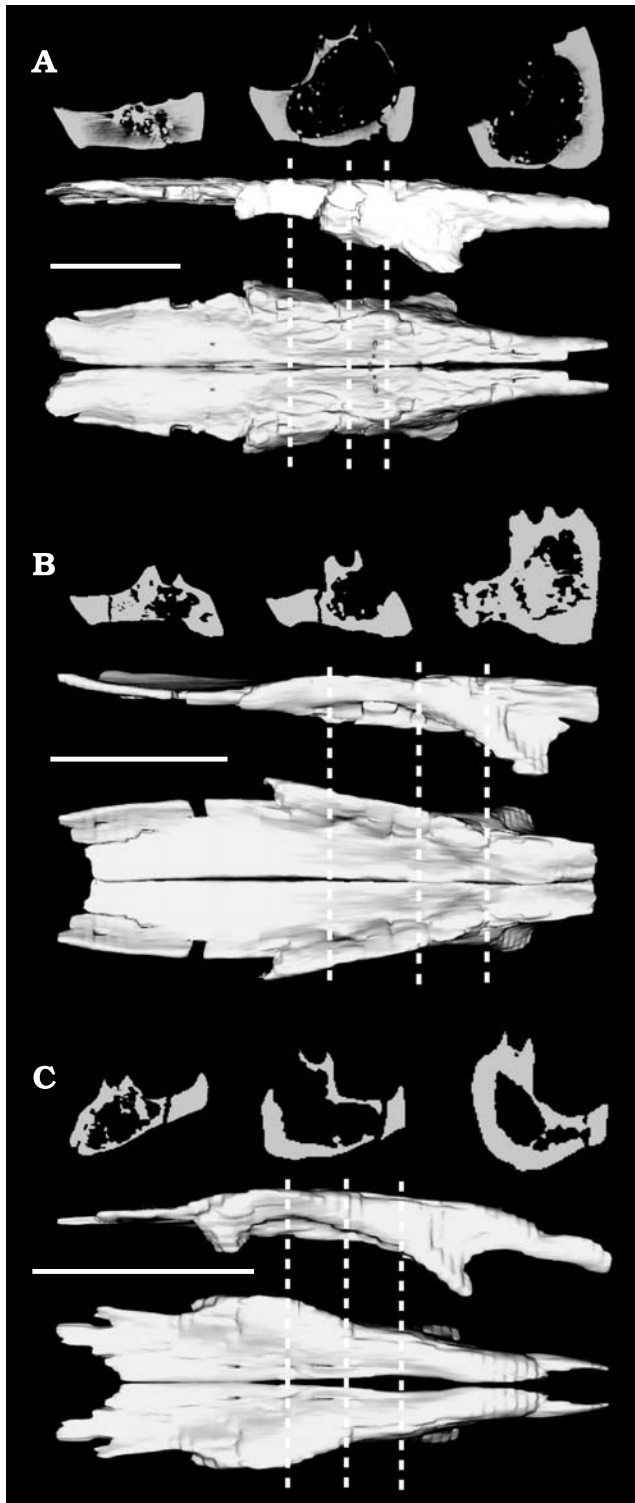


Fig. 5. CT cross sections and reconstructions of *Allosaurus fragilis* nasals: **A**, largest (UUV 1663/UMNH VP 9146); **B**, midsize (UUV 1913/UMNH VP 9144); and **C**, smallest (UUV 10854/UMNHVP 7784). Anterior is to the right. Cross sections are from the strongly pneumatized regions of the nasals, at positions indicated by the dashed lines. The slices are normalized to the same size to show the relative degree of pneumatic excavation, evident despite mineral infilling in some sections. Reconstructions are in lateral views and in dorsal views with single left or right specimens mirrored to replicate complete pairs. Specimen B is broken over the posterior part of the external nares. Scale bar 10 cm.

## Strengths of tyrannosaurid and *Allosaurus* nasals

### Materials and methods for examining theropod nasal strength

**Nasal specimens.**—Fossil nasal specimens included juvenile and adult specimens of *Gorgosaurus libratus*, and a larger adult specimen of *Gorgosaurus*'s sister taxon *Albertosaurus sarcophagus* (Fig. 4). These specimens are a tentative proxy for a nasal growth series of these tyrannosaurids, since the nasals share general morphological features (Currie 2003a) and the animals reach identical adult sizes (Currie 2003b).

We also scanned fossilized nasals of a large adult *Daspletosaurus torosus* and a high-resolution cast of nasals from its close relative *Tyrannosaurus rex* (Fig. 4). Scanning a cast to obtain cross-sections was appropriate for three reasons. Examination of the original specimen confirmed the fidelity of the cast, no other isolated *T. rex* nasal specimens were available, and cross-sectional geometry would be informative about strengths independently of internal architecture. A previous scan of a fossil *T. rex* skull (FMNH PR2081; Brochu 2003) demonstrated internal fusion of the nasals similar to that of other tyrannosaurids. We expect that the fossil template of our cast is internally similar to nearly all other tyrannosaurid nasals, and predict that CT sections of the fossil specimen (BHI 2033) would validate our strength calculations based on the cast.

We examined three individual left or right nasal specimens of the carnosaur *Allosaurus fragilis* (reconstructed and mir-

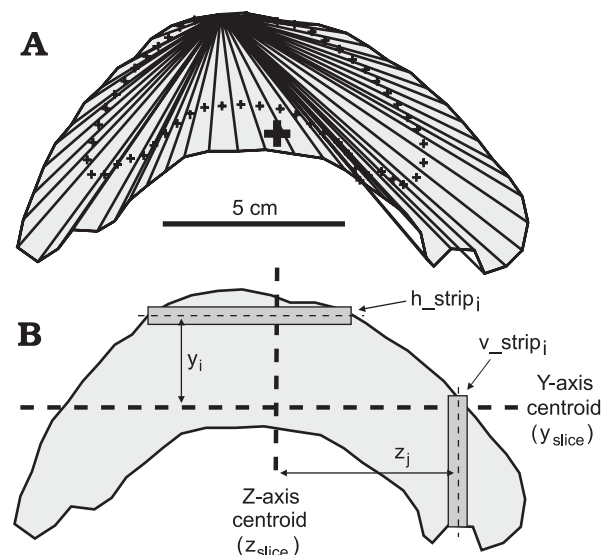


Fig. 6. Geometry used to compute the area, centroid, and second moments of area of a nasal cross-section (from middle region of fused *Tyrannosaurus rex* nasals: TMP 98.86.01; cast of BHI 2033). **A**. Decomposition of the cross-section to compute area by summing areas of triangles. Small "+" are centroids of individual triangles. Large "+" is the centroid for the complete section. **B**. Cross-section partitioned into horizontal and vertical strips of known area and position, used to calculate second moments of area.

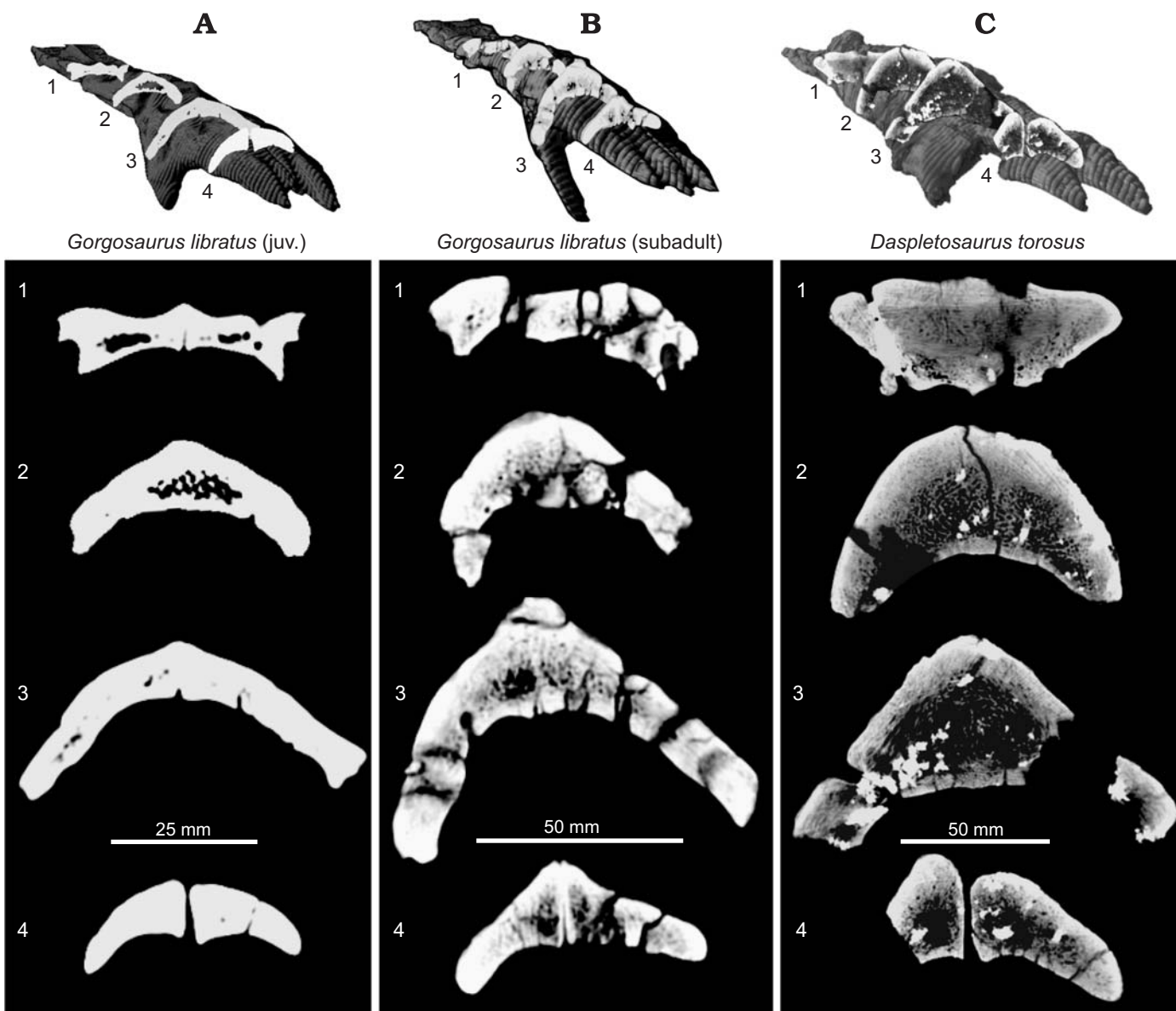


Fig. 7. CT-scanned cross-sections of fused tyrannosaurid nasals, showing greater vaulting and higher cross-sectional areas of bone in larger individuals. A. *Gorgosaurus libratus* (juvenile: TMP 86.144.1). B. *Gorgosaurus libratus* (subadult: TMP 86.64.1). C. *Daspletosaurus torosus* (adult: TMP 98.48.1). Numbers 1–4: cross-sections at topologically similar positions, from posterior to anterior.

rored to represent paired nasals: Fig. 5) from the collections of UUVF. These nasals represent a growth series of *A. fragilis* ranging in size from juvenile to adult, and overlap the size range of the smaller tyrannosaurids.

The specimens were CT scanned on a General Electric QX/1 scanner at Foothills Hospital, Calgary, Alberta. Scan settings of 120 KVp and 200 mA, at 5 mm thickness, produced good results. Thickness was reduced to 2.5 mm for the smaller *Gorgosaurus libratus* specimen.

**Specimen comparisons and CT data processing.**—CT slices were viewed to evaluate internal anatomy of the nasals in Madena X (<http://radonc.usc.edu/USCRadOnc/Madena/Madena.html>; Apple Macintosh OS X 10.3). Three-dimensional renderings (Figs. 1–3) and volume slicing for examin-

ing internal structure in context (Fig. 7) were performed in OsiriX (<http://homepage.mac.com/rossetantoinne/osirix/Index2.htm>; Apple Macintosh OS X 10.3). To test if our CT manipulations correctly visualized the internal structure of the bone, we examined naturally broken tyrannosaurid nasal specimens of varying size (TMP 81.23.1, 86.36.36, 92.36.81, 94.12.414, 94.154.2, 96.12.404).

The raw CT data were imported into ImageJ (<http://rsb.info.nih.gov/ij/>) where contrast enhancement, thresholding, particle analysis and other image processing commands (to fill holes, for example) were executed to produce filled regions corresponding to the nasal cross-sections. Subsequently, custom software was used to determine the (x,y) coordinates of the bone perimeters. The resolution of the finished contours is estimated to be 0.5 mm.

**Area calculations.**—With their positions along the top of the muzzle, the nasals are well positioned to receive the compressive forces associated with biting (Rayfield 2004), and their resistance to these forces will be proportional to their cross-sectional areas. The areas of the irregular nasal cross-sections were determined by the triangular decomposition method (Fig. 6) outlined in Henderson (2002).

**Strength calculations.**—Both nasals and skulls were represented in three-dimensional, Cartesian coordinate space, with posterior edges set at X = 0. The midsagittal axis was defined as the X-axis, and the dorsoventral axis was set to the Y-axis. The Z-axis defined the mediolateral axis, with negative and positive Z-coordinates correspond to left and right sides, respectively.

Determination of the horizontal and vertical neutral axes of bending of the nasal slices came from determining the Z- and Y-axis centroids (horizontal and vertical, respectively) of the contour bounded regions, and this was facilitated by the triangular decompositions used to determine areas (Fig. 6A) The centroid of the entire contour-bounded region ( $z$ ,  $y$ )<sub>slice</sub> is given by:

$$\begin{bmatrix} z \\ y \end{bmatrix}_{slice} = \frac{\sum_{n=0}^{N-1} \begin{bmatrix} z_n \\ y_n \end{bmatrix} \cdot A_n}{\sum_{n=0}^{N-1} A_n} \quad (1)$$

where N is the number of triangles in a contour decomposition, and ( $z_n$ ,  $y_n$ ) and  $A_n$  are the centroid and area, respectively, of the  $n^{\text{th}}$  sub-triangle (Appendix 2).

The second moments of area of a nasal cross-section with respect to the two axes were determined with the following expressions:

$$I_z^{nasal} = \sum_{i=0}^{I-1} \sum_{j=0}^{J-1} y_i^2 \cdot area(h\_strip_{(i,j)}) \quad (2)$$

$$I_y^{nasal} = \sum_{j=0}^{J-1} \sum_{i=0}^{I-1} z_j^2 \cdot area(v\_strip_{(j,i)}) \quad (3)$$

I and J are the numbers of horizontal and vertical slices,  $I_j$  and  $J_i$  are the numbers of separate strips on  $I^{\text{th}}$  horizontal and  $J^{\text{th}}$  vertical slices,  $y_i$  and  $z_i$  are the vertical and horizontal distances of strips from the centroid, and  $h\_strip$  and  $v\_strip$  are the areas of sets of individual strips taken in the vertical and horizontal directions, respectively (Fig. 6B).

**Influence of vaulting on tyrannosaurid nasals strengths.**—

We investigated the influence of vaulting on vertical strength by normalizing  $I_z$  for cross-sectional area of every tyrannosaurid CT slice, using the expression  $\bar{h}_{slice} = \sqrt{I_z^{slice} / A_{slice}}$ . The term  $\bar{h}_{slice}$  is the height of a rectangular cross-section, of area equal to that of the real slice ( $A_{slice}$ ), which would have a vertical second moment of area equal to that of the real slice ( $I_z^{slice}$ ). Dividing  $\bar{h}_{slice}$  by the length of the nasals converts  $\bar{h}_{slice}$  to a relative height, a dimensionless “vaulting index”, that al-

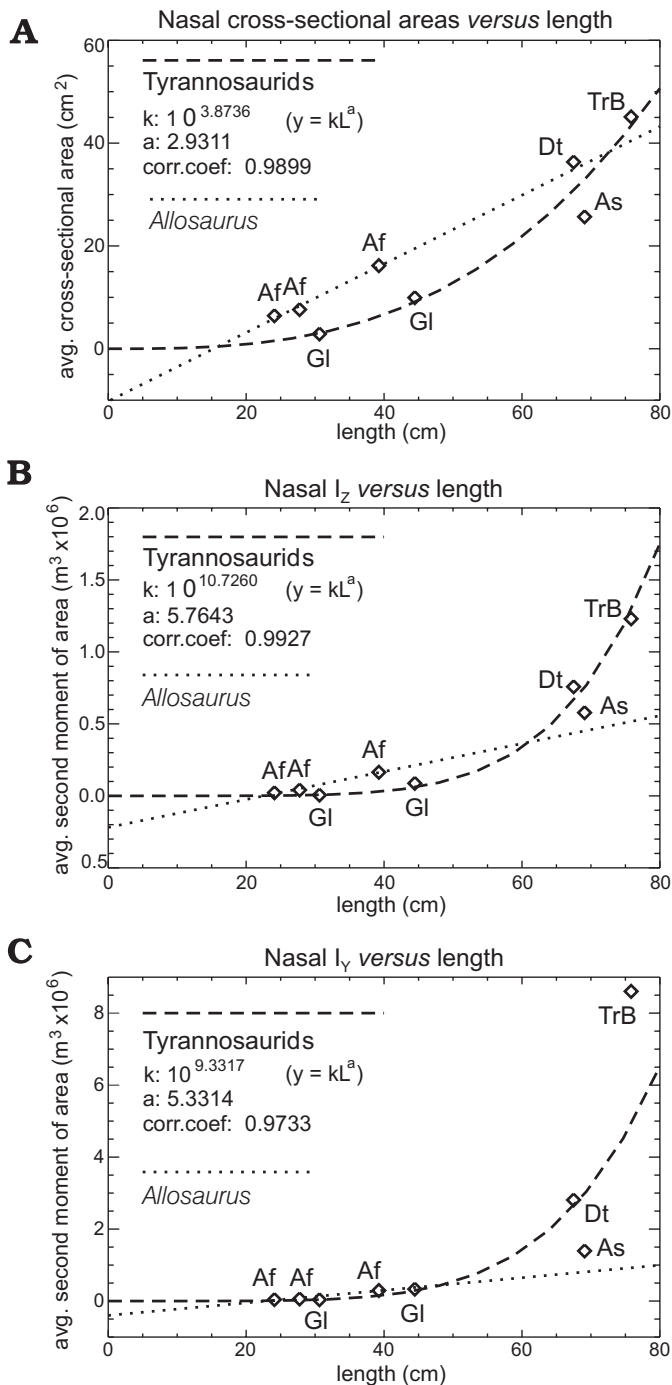


Fig. 8. Average strengths of nasal cross-sections in tyrannosaurids and *Allosaurus fragilis*, plotted against nasal length. **A.** Cross-sectional areas, proportional to compression strengths. **B.** Second moment of area, proportional to vertical bending strength. **C.** Second moment of area, proportional to lateral bending strength. Values for the *A. fragilis* nasals are uncorrected for the hollowness of the sections, which would reduce their strengths. Lines fitted to the tyrannosaurid values are derived from log transformed data. See Appendix 1 for labels.

lows comparison of the degree of vaulting between cross-sections of all taxa.

We also investigated the influence of allometry in nasal width on lateral strength by normalizing  $I_y$  for slice cross-

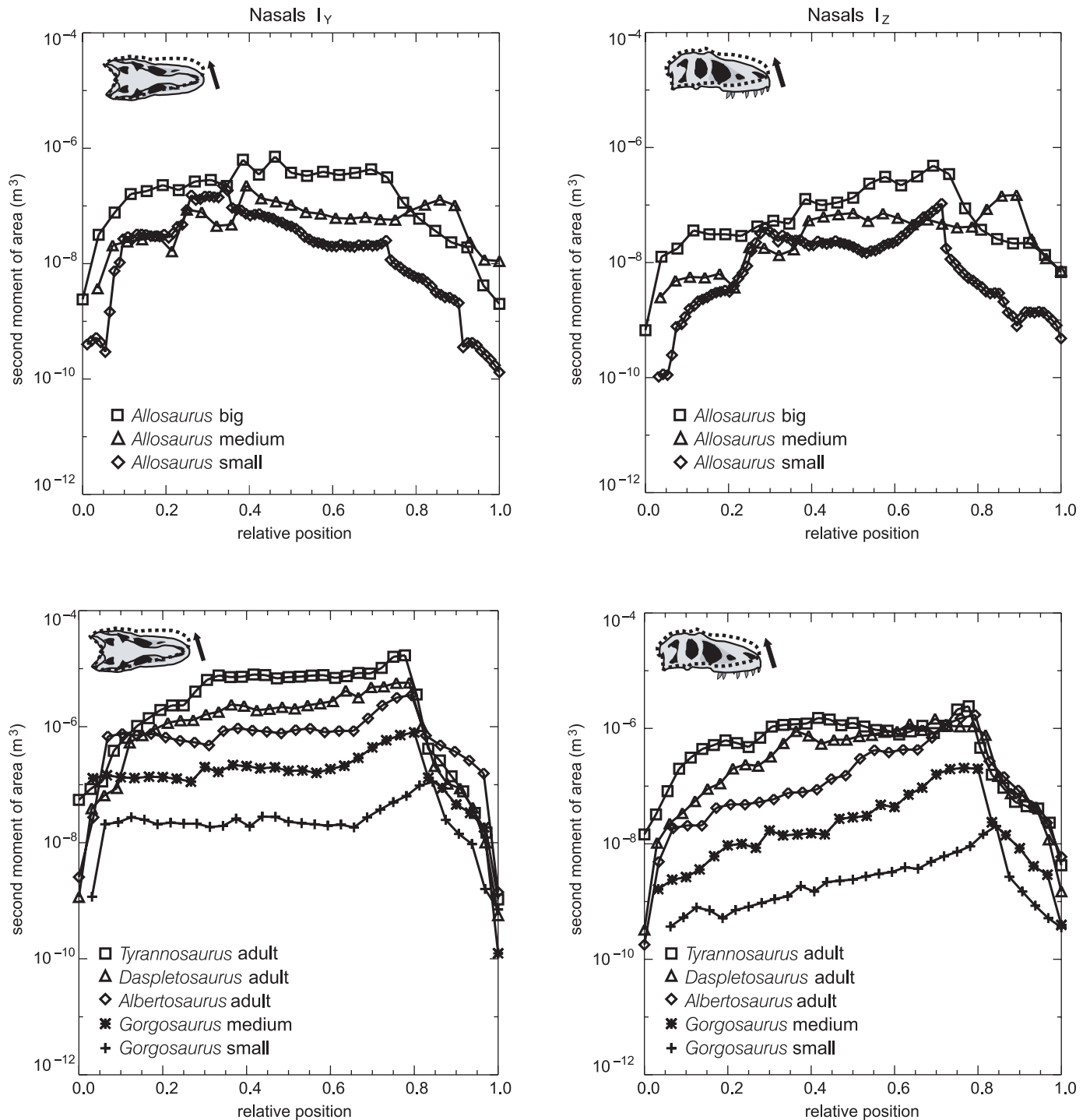


Fig. 9. Comparison of theropod nasal strengths at multiple transverse sections. Horizontal ( $I_y$ ) and vertical ( $I_z$ ) second moments of area of nasal cross-sections of *Allosaurus fragilis* (upper two graphs) and tyrannosaurids (lower two graphs). Second moments of area are proportional to lateral ( $I_y$ ) and vertical ( $I_z$ ) bending strengths. X-axes of graphs show relative position of slices along the long axes of the bones: 0.0 is posterior and 1.0 anterior.

sectional area. By the expression  $\bar{s}_{slice} = \sqrt{I_y^{slice} / A_{slice}}$ ,  $\bar{s}_{slice}$  is the span (width) of a rectangle of area equal to  $A_{slice}$ , that would have the same lateral second moment of area as the real slice. Dividing  $\bar{s}_{slice}$  for every slice by the lengths of their respective nasals yields a dimensionless “span index” for the contribution of slice widths to  $I_y^{slice}$ .

### Results of nasal morphology and strength analyses

Fig. 7 depicts several CT cross-sections through selected tyrannosaurid nasals. All are minimally fused to unfused anteriorly, strongly fused and vaulted in the middle sections, and

Table 2. Computed strength properties of theropod nasals.

	Length (cm)	$I_z$ ( $m^4 \times 10^{-8}$ )	$I_y$ ( $m^4 \times 10^{-9}$ )	Avg. Cross-Sectional Area ( $m^2 \times 10^{-4}$ )
<i>Gorgosaurus libratus</i> (juvenile) (Gl)	31.0	2.935	3.515	2.335
<i>Gorgosaurus libratus</i> (subadult) (GI)	46.5	21.94	45.55	7.709
<i>Albertosaurus sarcophagus</i> (As)	68.7	93.30	302.6	19.44
<i>Daspletosaurus torosus</i> (Dt)	68.0	187.5	519.0	27.69
<i>Tyrannosaurus rex</i> (Tr)	81.0	496.3	769.7	33.30
<i>Allosaurus fragilis</i> (small) (Af)	24.1	3.881	17.01	4.376
<i>Allosaurus fragilis</i> (medium) (Af)	28.0	7.186	45.53	6.725
<i>Allosaurus fragilis</i> (large) (Af)	40.5	24.62	115.3	13.04

flatter posteriorly. Cortical bone was extensive, and the struts comprising the spongy bone in the nasals' interiors were so densely packed that they were only clearly visible under high contrast in the CT images. Observations of naturally broken specimens corroborate that the high density apparent in CT slices was not an artifact of inaccurate visualization. CT slices of larger specimens appear proportionally more highly vaulted, wider relative to the element's length, and consequently more robust than in the juvenile *Gorgosaurus libratus* specimen (Fig. 7A). The *Daspletosaurus torosus* specimen (Fig. 7C) appears especially massive and tall in cross section.

Nasal cross-sectional areas, which correlate positively with compressional strength (Gordon 1979), are much higher in the adult tyrannosaurids than in other specimens (Table 2, Fig. 8). Areas for *Daspletosaurus torosus* are higher than in the *Albertosaurus sarcophagus* nasals of the same length.

Table 2 reports average second moments of area  $I_z$  and  $I_y$ , which respectively indicate vertical and lateral bending strengths, and average cross-sectional area, for all examined tyrannosaurid and *Allosaurus* nasals. The average  $I_z$  for resistance to vertical bending increases faster than nasal length. While lateral strength indicators  $I_y$  are not as high as those for vertical bending, the discrepancies between small and large specimens are even more dramatic (Table 2).

The *Daspletosaurus* and *Tyrannosaurus* nasals had higher average indicators for vertical bending strength than in the adult *Gorgosaurus* and *Albertosaurus*.  $I_y$  of the *Daspletosaurus* nasals is almost twice that of the equivalently long adult *Albertosaurus* specimen (Fig. 8). The *Allosaurus* nasals had relatively high strength indicators  $I_y$  and  $I_z$  for bending when compared with tyrannosaurid nasals of a given length (Fig. 8), although their increases in nasal bending strength with increases in nasal length are less dramatic than in the tyrannosaurids.

Fig. 9 graphs the distribution of second moments of area for individual nasal cross-sections. For resistance to vertical bending *Allosaurus* and tyrannosaurid nasals have higher  $I_z$  anteriorly than posteriorly. At posterior sections in *Gorgosaurus* and *Albertosaurus*,  $I_z$  falls off more rapidly than in *Tyrannosaurus* and *Daspletosaurus*. Resistance to lateral bending  $I_y$  generally increases posteriorly in *Allosaurus*. The lateral strength indicators peak anteriorly in tyrannosaurids, and in general decrease posteriorly.

In all specimens the anterior- and posteriormost second moments of area are low. Other bones articulate with the nasals in these areas, however, and presumably compensate for low strengths here of the nasals themselves (Figs. 5, 7, 8).

Our "vaulting index" measures the effects of shape on nasal strength (Fig. 10A), and shows that the vertical second moment of area would be greater in the adult tyrannosaurids, even if corresponding slices in all tyrannosaurid specimens were scaled to the same cross sectional areas. Above the largest maxillary teeth, the adult *Albertosaurus*, *Daspletosaurus*, and *Tyrannosaurus* nasals are more highly vaulted than in the juvenile *Gorgosaurus*. The subadult *Gorgosaurus* specimen approaches the degree of vaulting seen in the adult *Albertosaurus*, possibly indicating that the nasals of these taxa increased little in vaulting after a certain stage of growth. Posteriorly the *Daspletosaurus* and *Tyrannosaurus* nasals are more vaulted than in the other taxa, and which may have contributed to greater relative bending strength of these elements.

The "span index" (Fig. 10B) indicates that allometric expansion in width had little effect on lateral second moment of area  $I_y$  for most of the tyrannosaurids, because their area-normalized scores for  $I_y$  overlap. However,  $I_y$  values of the anterior *Tyrannosaurus rex* cross-sections were much higher than in the other taxa, indicating that allometric lateral expansion increased the relative lateral bending strength of its nasals.

## Cranium strengths of tyrannosaurids and carnosaurus

### Materials and methods for calculating theropod cranium strength

**External geometry of theropod crania.**—We produced 3D numerical representations of theropod crania (Fig. 11) in order to examine the correspondence between cranium shape and strength. We chose tyrannosaurid and carnosaur specimens of similar skull lengths, approximately matching the tyrannosaurids *Gorgosaurus libratus*, *Daspletosaurus torosus*, and a medium sized *Tyrannosaurus rex* with the carnosaurus *Allosaurus fragilis*, *Sinraptor dongi*, and *Acrocanthosaurus atokensis*, respectively.

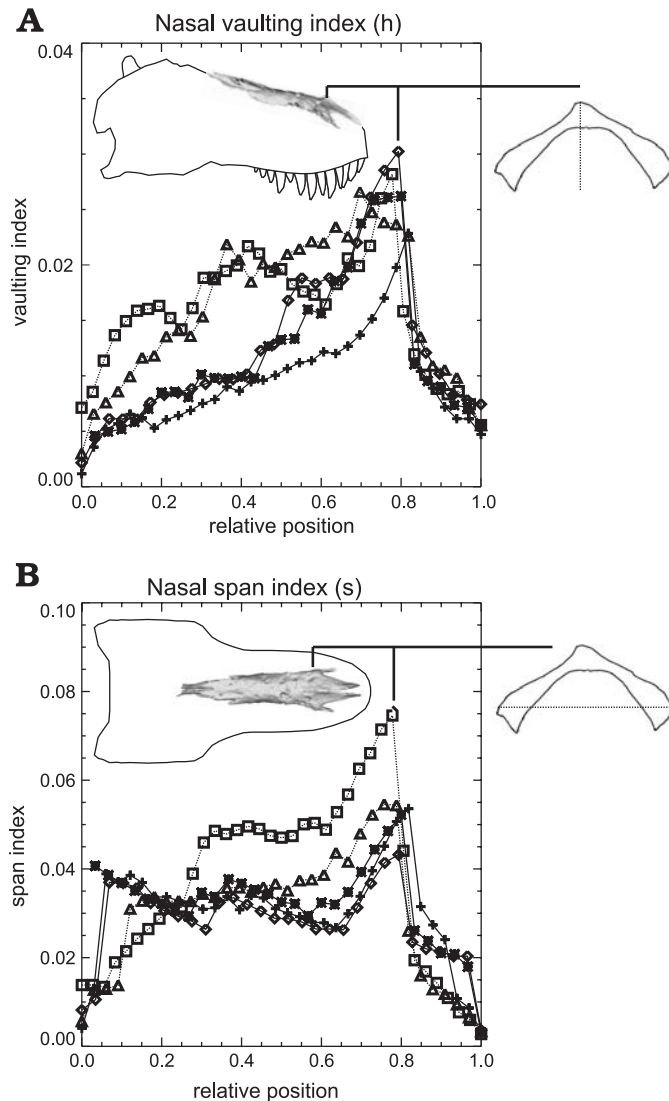


Fig. 10. Heights and widths of tyrannosaurid nasal slices normalized for slice area and bone length. **A.** Normalized heights (“vaulting index”) showing convergence of vaulting pattern at large size. **B.** Normalized widths (“span index”) showing isometric form in most specimens, but exaggerated relative width in *Tyrannosaurus rex* nasals. Points of maximum vaulting and span are indicated on nasals of *T. rex* (TMP 98.86.01; cast of BHI 2033). Symbols as per Fig. 9.

To encompass the upper end of the theropod size range, we reconstructed the cranium of a large *Tyrannosaurus rex* (1.4 m; FMNH PR2081) and the similarly huge *Carcharodontosaurus saharicus* (1.6 m; SGM-Din 1). The larger *Tyrannosaurus rex* cranium (FMNH PR2081) was crushed during fossilization, but we were able to reconstruct it based on measurements in its description (Brochu 2003) and comparisons with other *T. rex* crania. The *C. saharicus* cranium (SGM-Din 1) lacks the premaxilla but the specimen’s width and height are known. Because bending and torsional strength scale linearly with length but with the square of width and height, a different length than restored for the *Carcharodontosaurus* cranium by Sereno et al. (1996) would have a relatively minor effect on the specimen’s strength indices.

**Data collection for cranium geometry.**—Isometric dorsal and lateral images of the crania from published illustrations were scanned on a flatbed scanner, and the dorsal and lateral profiles of the crania were traced in Canvas 7 (Deneba Software Inc.; Fig. 11). The bending and torsional strengths of a cranium depend on its transverse cross-sectional shapes, and on how these shapes vary along the cranium’s length. All the crania were therefore represented in mathematical form as sets of horizontally stacked, transverse, two-dimensional plinges (flat-topped corbelled vaults: Gordon 1984; Figs. 8, 9). Unlike the strong nasals, the crania of most dinosaurs are found in slightly to very distorted states (e.g., the American and Field Museum *Tyrannosaurus rex* specimens, respectively). This leads to uncertainty regarding the exact form of the original uncrushed cranium. With the nasals, their original geometry is well preserved and it was felt worthwhile to use precise CT methods to capture their shape. In contrast, the uncertainties of cranial preservation made a first order approximation adequate for our purposes.

**Area calculations.**—Calculating areas of cranium plinge sections is fundamental, as all other mechanical properties of the cranium depend on the areas in some way. All theropod crania have a typical form that results in all transverse slices being laterally symmetrical quadrilaterals (“trapezoids”) with a ventral (lower) edge that is wider than the accompanying dorsal (upper) edge (Fig. 9). The areas of these trapezoidal cross-sections, and excised areas representing the interior of each plinge (see below), were computed using the method outlined in Henderson (2002).

**Strength calculations.**—Dorsoventral and mediolateral modes of bending are relevant to the study of the cranium mechanics of predatory dinosaurs. In each mode the side of the cranium where a force is being applied will experience tension, while the opposite side will be in compression. Somewhere between the compressed and tensed sides is an infinitesimally thin zone, the neutral axis, that does not experience any stress. For dorsoventral bending this neutral axis is equivalent to the horizontal,  $y$ -axis centroid,  $\bar{y}$ . As the crania and their transverse slices are left-right symmetrical, the central  $Y$ -axis ( $Z = 0$ ) is the neutral axis for mediolateral bending.

A cranium’s bending strength at a particular point depends on two parameters—the second moment of area of the corresponding cross-section, and its distance from the point of force application. The first parameter is a measure of how the material comprising the slice is distributed about the neutral axis of the slice (Gordon 1978). For dorsoventral bending this quantity,  $I_z^{skull}$ , is computed relative to the horizontal  $Z$ -axis, and is expressed as:

$$I_z^{skull} = \int_{y_t}^{y_c} y^2 dA \quad (4)$$

where  $y_c$  and  $y_t$  are the distances from  $\bar{y}$  to the top and bottom edges of the cross-section that experience compression and

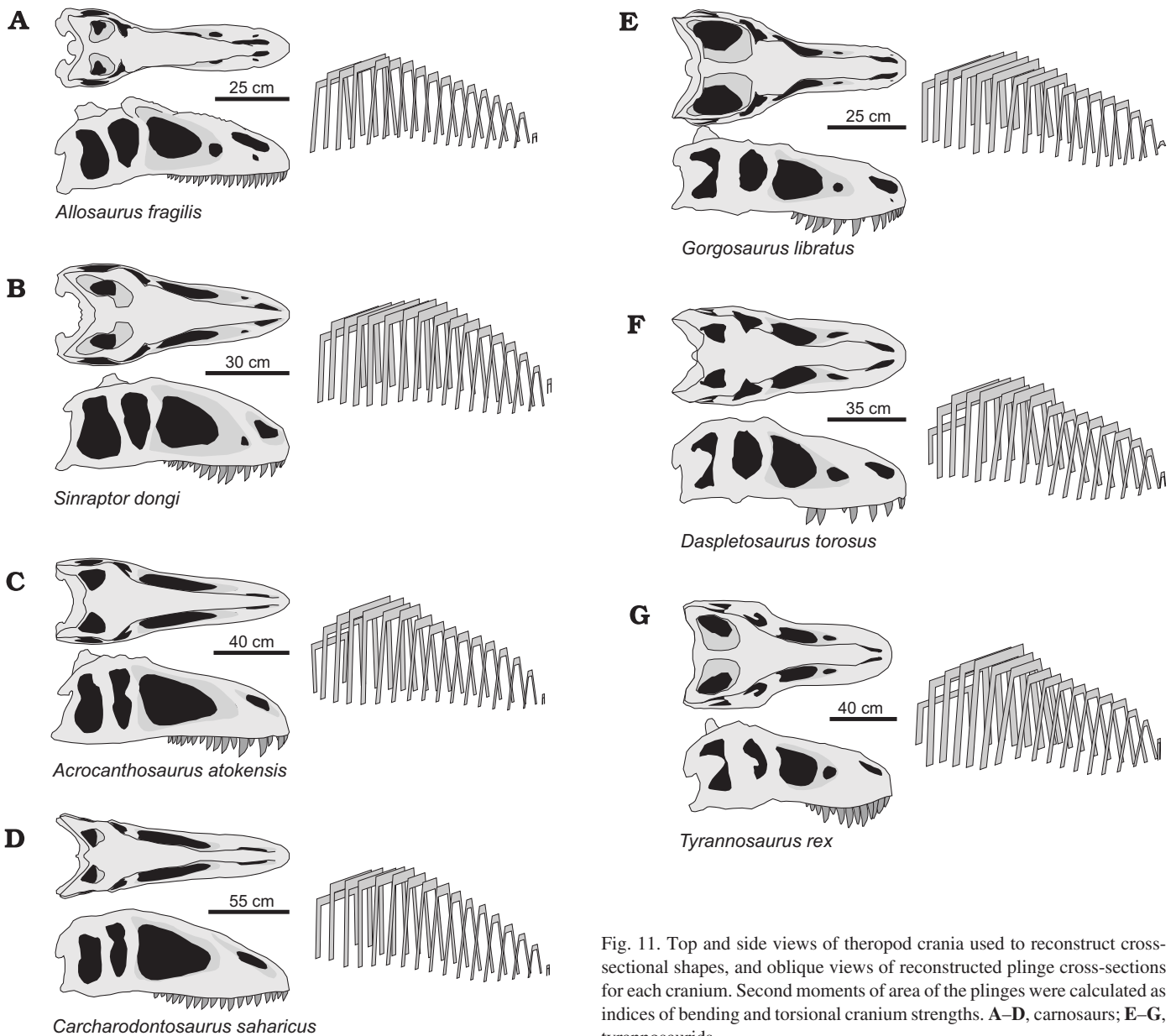


Fig. 11. Top and side views of theropod crania used to reconstruct cross-sectional shapes, and oblique views of reconstructed plinge cross-sections for each cranium. Second moments of area of the plinges were calculated as indices of bending and torsional cranium strengths. A–D, carnosaurs; E–G, tyrannosaurids.

tension, respectively, and  $dA$  is a horizontal strip of area that will vary with height (Fig. 12A). For a theropod biting prey, and with the impact force directed upwards, the dorsal side of the cranium will be under compression and the ventral side under tension.

For mediolateral bending the expression for second moment of area with respect to the vertical axis,  $I_y^{skull}$ , is given by:

$$I_y^{skull} = 2 \cdot \int_{z=0}^{z_D} z^2 \cdot (y_D - y_V) dz + 2 \int_{z=z_D}^{z_V} z^2 [m_{lateral}(z - z_D) + y_D - y_V] dz \quad (5)$$

where the first term is for a rectangular region immediately adjacent to the central, vertical neutral axis, which is bounded

vertically by  $y_D$ , and  $y_V$ , and laterally by  $z_D$  (Fig. 12B). The second term is for a laterally positioned triangular region which is bounded along its top edge by the lateral side of the plinge, and extends along its lower edge to  $z_V$ . To account for the left-right symmetry of the trapezoidal shape each term is multiplied by two.

The above expressions for second moments of area are for solids, but crania are not solid blocks of bone. To represent for the hollowness of the cranial vault, a second inner shell was defined. The mean thickness of bones comprising a cranium was estimated to be 5% of the cranium length. This thickness was subtracted from the dimensions defining the outer cranium contours, with the original and reduced trapezoids sharing the same bottom edge. Second moments of area were computed for the reduced internal cranium shapes, and the resulting values were subtracted from second mo-

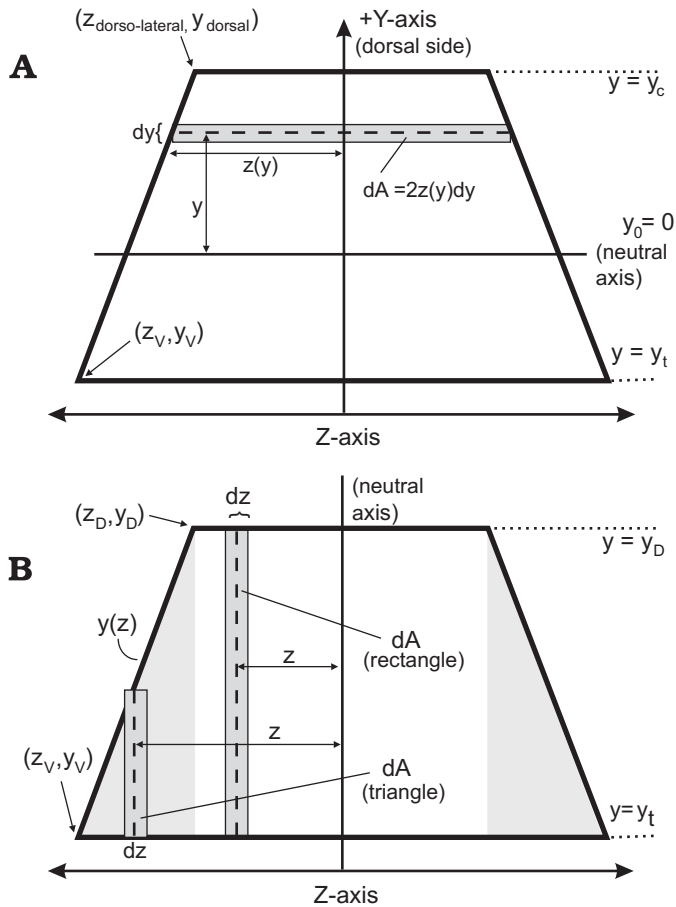


Fig. 12. Schematic trapezoidal cross-sections of theropod crania, with geometry and expressions for computing second moments of area. **A.** Determining moments with respect to the horizontal (Z) axis. The width of a strip of area is a function of its vertical (Y) coordinate. **B.** Determining moments with respect to the vertical (Y) axis; the cross-section is partitioned into two central rectangular areas, and two lateral triangular regions.

ments of area of the original, external geometries following the methods of Farlow et al. (1995). We used the mean of the second moments of area all the slices as a strength indicator for the cranium as a whole. This was appropriate for our present interest in correlations between nasal bone strengths and general cranium strengths.

In addition to the two modes of bending deformation, there is also the potential for the torsional deformation as the cranium twists about its long axis during feeding activities. The torsional strength of the cranium is proportional to the polar second moment of area ( $J$ ). For each cranium slice,  $J$  was computed as the sum of the two orthogonal second moments of area,  $I_z$  and  $I_y$  (Biewener 1992). The mean value  $J$  for all the slices was then assigned to the cranium.

### Cranial strength results

The results in Fig. 13 and Table 3 show that tyrannosaurid crania had generally higher second moments of area and higher torsional strength indicators than carnosaur crania of equivalent length. Tyrannosaurid cranium geometry there-

fore conferred generally higher strength in torsion and in lateral and dorsoventral bending. The results for *Tyrannosaurus rex* amplify the trend towards higher strengths in tyrannosaurids than in carnosaurids. The smaller *T. rex* cranium (TrA) shows approximately twice the dorsoventral bending and torsional strengths, and three times the medio-lateral bending strength, of the equally long cranium of *Acrocanthosaurus atokensis* (Aa). This *T. rex* cranium had higher torsional and lateral bending strength indicators than the much longer cranium of *Carcharodontosaurus saharicus* (Cs). The larger *T. rex* cranium TrF is 12.5% longer than the smaller TrA, but its substantially higher strength reflects the non-linear increase in second moment of area with increasing linear size (equations 4 and 5).

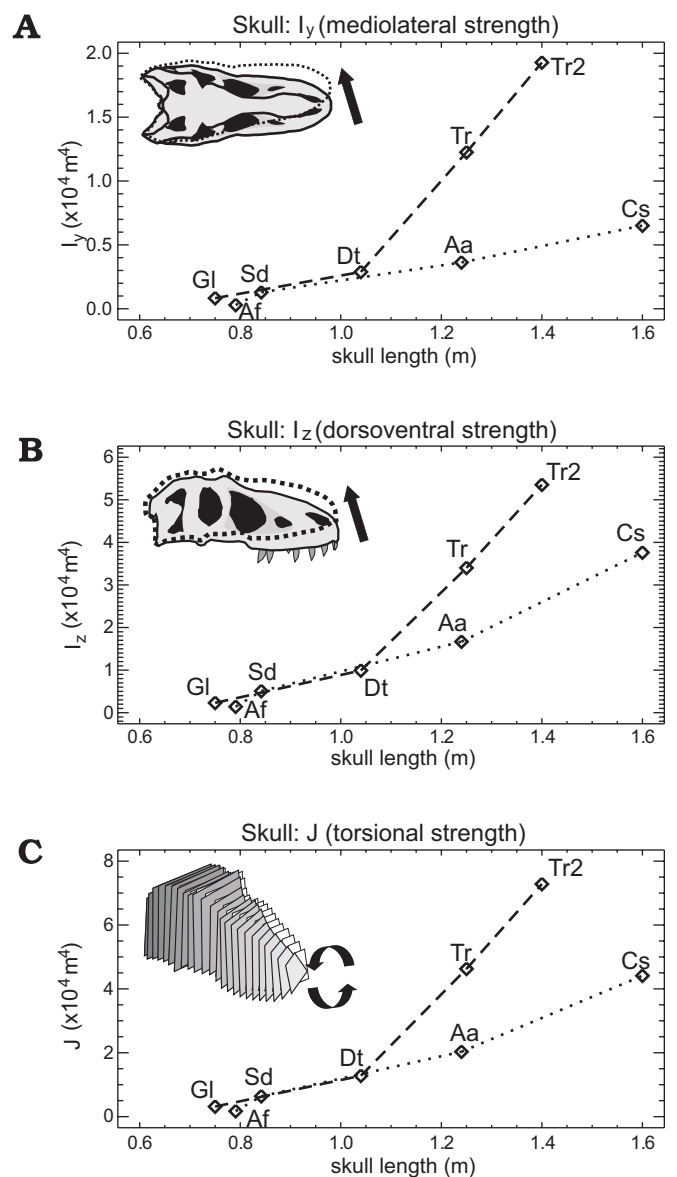


Fig. 13. Strength indicators computed for theropod crania under medio-lateral (A), dorsoventral (B), and torsional (C) loadings. Tyrannosaurid crania are invariably stronger than those of carnosaurids for a given skull length. See Appendix 1 for labels.

## Discussion

### Are hypotheses of tyrannosaurid tooth, nasal and cranial strength validated?

#### Tyrannosaurid maxillary teeth were stronger in bending than those of other large carnivorous dinosaurs.—

This hypothesis is partly falsified in that the average maxillary tooth strengths of most tyrannosaurids are not substantially higher than those of carnosaurs at equivalent skull lengths. The teeth of the carnosaur *Sinraptor dongi* are notably robust; while not as thick at the base as most tyrannosaurid teeth they have lower crown heights and low bending moments arms. However, tyrannosaurid teeth vary more in size along the maxillary row than in other theropods, and the strengths of the largest maxillary tooth tend to be higher in tyrannosaurids relative to skull length. The average and maximum tooth strengths of *Tyrannosaurus rex* are much higher than those of non-tyrannosaurids when normalized for skull size. High mediolateral bending strength of *T. rex* teeth corresponds with Meers' (2003) observation that *T. rex* rostra were broader than the mediolateral span of the dentaries. If the animals bit into bone often and food was caught between the tooth rows, this jaw arrangement would impose lateral bending forces on the maxillary teeth and medial forces on the dentary teeth. A high mediolateral section modulus would reduce stress that these forces imposed on the teeth.

The trends of increase in tooth strength with skull length are markedly different between tyrannosaurids and other large theropods. The high strengths of *Tyrannosaurus rex* teeth contribute to the non-linear trend in the tyrannosaurids. The particularly strong maxillary teeth of *T. rex* are consistent with high bite forces (Erickson et al. 1996) and mandible strength (Therrien et al. 2005) found for this taxon, and indicate that its feeding apparatus was stronger than expected for a tyrannosaurid its size.

#### Vaulting contributed significantly to tyrannosaurid nasal strength.—

The nasal "vaulting index" (Fig. 10A) indicates that the vertical second moments of area in large tyrannosaurids is higher than expected if they retained the same cross-sectional shapes of the smaller specimens. Thus vaulting of the nasals, more than increased cross-sectional area, increased their second moments of area and strengths of large tyrannosaurid nasals in bending and torsion. We predict that analysis including more juvenile specimens will uphold these findings. Our "span index" (Fig. 10B) shows that anterior broadening of the nasals in the *Tyrannosaurus rex* specimen increased its lateral bending strength in this region.

#### Fused tyrannosaurid nasals were stronger than unfused carnosaur nasals.—

Our results for the geometric contributions to nasal strength artificially exaggerate the strengths of the *Allosaurus fragilis* nasals, and diminish those of *Gorgosaurus libratus* and *Albertosaurus sarcophagus*. The computed average strengths of *Allosaurus fragilis* nasals are

Table 3. Computed strength properties of theropod crania.

	Length (cm)	$I_z$ ( $m^4 \times 10^{-5}$ )	$I_y$ ( $m^4 \times 10^{-6}$ )
<i>Allosaurus fragilis</i> (Af)	79.1	1.411	2.975
<i>Sinraptor dongi</i> (Sd)	84.2	5.083	12.93
<i>Acrocanthosaurus atokensis</i> (Aa)	124	16.68	36.26
<i>Carcharodontosaurus saharicus</i> (Cs)	160	37.61	65.11
<i>Gorgosaurus libratus</i> (Al)	75.0	2.304	8.296
<i>Daspletosaurus torosus</i> (Dt)	104	9.911	28.85
<i>Tyrannosaurus rex</i> (TrA)	125	34.02	122.5
<i>Tyrannosaurus rex</i> (TrF)	140	53.53	192.8

higher than those of the albertosaurine tyrannosaurids when plotted against nasal length (Fig. 8). However, averages for the albertosaurine tyrannosaurid nasals are reduced by strength properties of their flat caudal projection, where articulating bones would augment the nasal strengths. The anterior, vaulted portions of the albertosaurine nasals, where they would receive the brunt of forces from the maxillae, have higher strengths than the *A. fragilis* nasals (Fig. 9). Also, pneumaticity of the *A. fragilis* nasals (Fig. 5) would reduce their strengths somewhat. The average compressional strengths would decrease by approximately 30%, and second moments of area by approximately 6%

The extensive fusion seen in tyrannosaurid CT sections would increase their torsional and compressive strengths, with benefits for feeding function. Tooth marks show that large theropods applied powerful bites that cut bone (Chure et al. 2000). With unilateral biting, unfused nasals would experience vertical shear between left and right halves, causing dorsal displacement of one side of the snout relative to the other and straining ligaments that connected the nasals. In tyrannosaurids, fusion added bone to the midline of the nasals where the structures are notably tall in cross-section (Fig. 6). Because shear strength is proportional to the dimension of a structure parallel to shear forces, increased height of bone along the midline would resist dorsoventral shear.

The combination of fusion and high second moments of area gave the dorsal portion of tyrannosaurid nasals the properties of a torsion tube resistant to twisting forces (similar to the entire muzzles of crocodylians: Busbey 1995). With bone rather than ligaments resisting the tensile components of shear and torsion, and bone resisting compressive torsional components, the food would have experienced a greater proportion of the full bite force in tyrannosaurids than in carnosaurs.

High proportions of bone in cross-sections of tyrannosaurid nasals indicate higher compressional strength than the collective strength of *Allosaurus* nasals. CT sections (Fig. 5; Emily Rayfield, personal communication 2004) and openings into the bones (Witmer 1997) show that *Allosaurus* nasals were hollowed out through much of their length (Fig. 5) by pneumatizing tissues, reducing their cross-sectional area and compressive strength. In contrast, CT sections and broken fossilized specimens show that tyrannosaurid nasals had exten-

sive cortical bone, high densities of trabecular bone, and small vascular canals (Currie 2003a) but no pneumatic cavities.

**Tyrannosaurid crania were stronger overall than carnosaur crania.**—The results confirm that tyrannosaurid crania were stronger than those of other theropods of similar skull length (Table 3). The *Gorgosaurus libratus* cranium was minimally 1.5 times stronger (in vertical bending) than a slightly longer cranium of *Allosaurus fragilis*. The *Tyrannosaurus rex* crania were much stronger than equivalently sized or larger carnosaur crania, except for a modestly higher vertical bending indicator for *Carcharodontosaurus saharicus* versus the smaller *T. rex* specimen.

### Pattern of correlated progression of tyrannosaurid feeding mechanics

Thomson's (1966) concept of correlated progression involves the evolutionary integration of adaptive features (Fig. 14A). Structural modifications of the tyrannosauroid feeding apparatus suggest integration of faculties towards reduction of large prey. We adopt the phrase "correlated progression" with the caveat that it does not imply universal adaptive improvement. Escalating performance in one area may lead to loss of capability in others, such as a reduced ability of the adults of larger predators to capture smaller prey.

Correlated progression is testable by examining correspondences between rates of performance increase for various structures. The nasals, teeth, dentaries, and crania of tyrannosaurids show consistent patterns of positive allometric increase in strength when plotted against cranium or dentary length (Figs. 2, 3, 8, 13). In contrast, elements of other large theropods show linear increases in strength with increasing skull size (Figs. 2, 3, 8, 13).

The tyrannosaurid trends reveal a more complex, mosaic pattern of correlated progression than lock-step increases in strength for all structures. With most comparable structures, adult tyrannosaurine taxa (*Daspletosaurus torosus* and *Tyrannosaurus rex*) have higher size-normalized strengths than the albertosaurine forms, and *T. rex* in turn has higher strengths than *D. torosus*. Because these taxa represent successively more derived forms (Holtz 2004), similar patterns of strength increase for all examined structures support the hypothesis of correlated progression of the tyrannosaurid feeding apparatus (Fig. 14B). However, the adult *D. torosus* maxillary teeth are no stronger than those of the *Albertosaurus* specimen, while *T. rex* maxillary teeth are much stronger than either. Rather than showing an insensibly continuous trend, the allometric increase for maxillary teeth probably reflects a quantum jump in strength from the condition in *Albertosaurus* and *Daspletosaurus* to that of *T. rex*. The more gradual increase in nasal and cranial strengths indicates that robustness of these structures preceded acquisition of particularly strong teeth in adult *T. rex* (Fig. 14B). If the giant *Tarbosaurus bataar* experienced a "growth spurt" similar to that of *T. rex* (Erickson et al. 2004), its narrower skull

(Hurum and Sabath 2003) indicates that it may have continued the ontogenetic trajectory of strength increase seen in smaller tyrannosaurids. *T. rex*, in contrast, probably experienced greater hypermorphosis of tooth and cranial strengths during this growth period.

Tooth, nasal, and cranial strengths likely increased in parallel with jaw adductor forces. Bite forces were probably enhanced in tyrannosaurids through enlarged muscle origins from midsagittal and nuchal crests (m. adductor mandibulae externus medialis) and perhaps the expanded quadratojugal-squamosal contact (Molnar 1973), and increased size of the adductor chamber. These trends in feeding strengths are elucidated by consideration of how tyrannosaurid nasals contributed to cranium strength, and possible behavioural consequences of skull strengths in theropods.

### Mechanical integration of theropod nasal and cranium strengths

Our results for nasal compressional strength support Rayfield's (2004) hypothesis that the nasals strengthened the cranium in vertical bending. Rayfield (2004) ran a finite element analysis of the skull of *Tyrannosaurus rex* (BHI 2033, the specimen that was cast for our *T. rex* nasals: TMP 98.86.01) as a plate-like lateral projection. With the joints between ventral cranium bones treated realistically as unfused, the model showed high compressional stress over the anterior maxillary teeth (as predicted by Molnar 1973, 2000). This is precisely where *Tyrannosaurus rex* nasals, and those of other tyrannosaurids, show the highest cross-sectional areas. With a large cross-sectional area the nasals could withstand high compressional forces, such as those incurred during dorsal bending of the rostrum, without experiencing unusually high stress.

Adult specimens *Tyrannosaurus rex*, and similarly gigantic adults of the tyrannosaurid *Tarbosaurus bataar*, have staircase-style interdigitating sutures, with triangular pegs and sockets, between the nasals and maxillae (Hurum and Sabath 2003; Rayfield 2004; Fig. 15). This staircasing does not occur in a juvenile specimen of *Tarbosaurus bataar* (TMP 2000.50.5; cast), or in adults of other examined tyrannosaurids (including the large, robust *Daspletosaurus torosus* specimen). This additional reinforcement of the nasal-maxillary suture may be exclusive to adult *Tarbosaurus* and *Tyrannosaurus*, and related to increased feeding forces involved with engaging larger prey (see below).

Rayfield (2004) noted that nasal-maxilla interlocking would brace the joint against high concentrations of shear stress in the region between the nasals and maxillae of *Tyrannosaurus rex*, and efficiently channel compressive biting stress from the maxillae to the nasals. The staircasing would also brace the joints against shear induced by lateral bending and torsion of the snout, and complement high nasal and rostrum strengths found for *T. rex*.

High second moments of area of the tyrannosaurid nasals relative to those of *Allosaurus fragilis* demonstrate higher strength of the dorsal part of the snout, and emphasize how

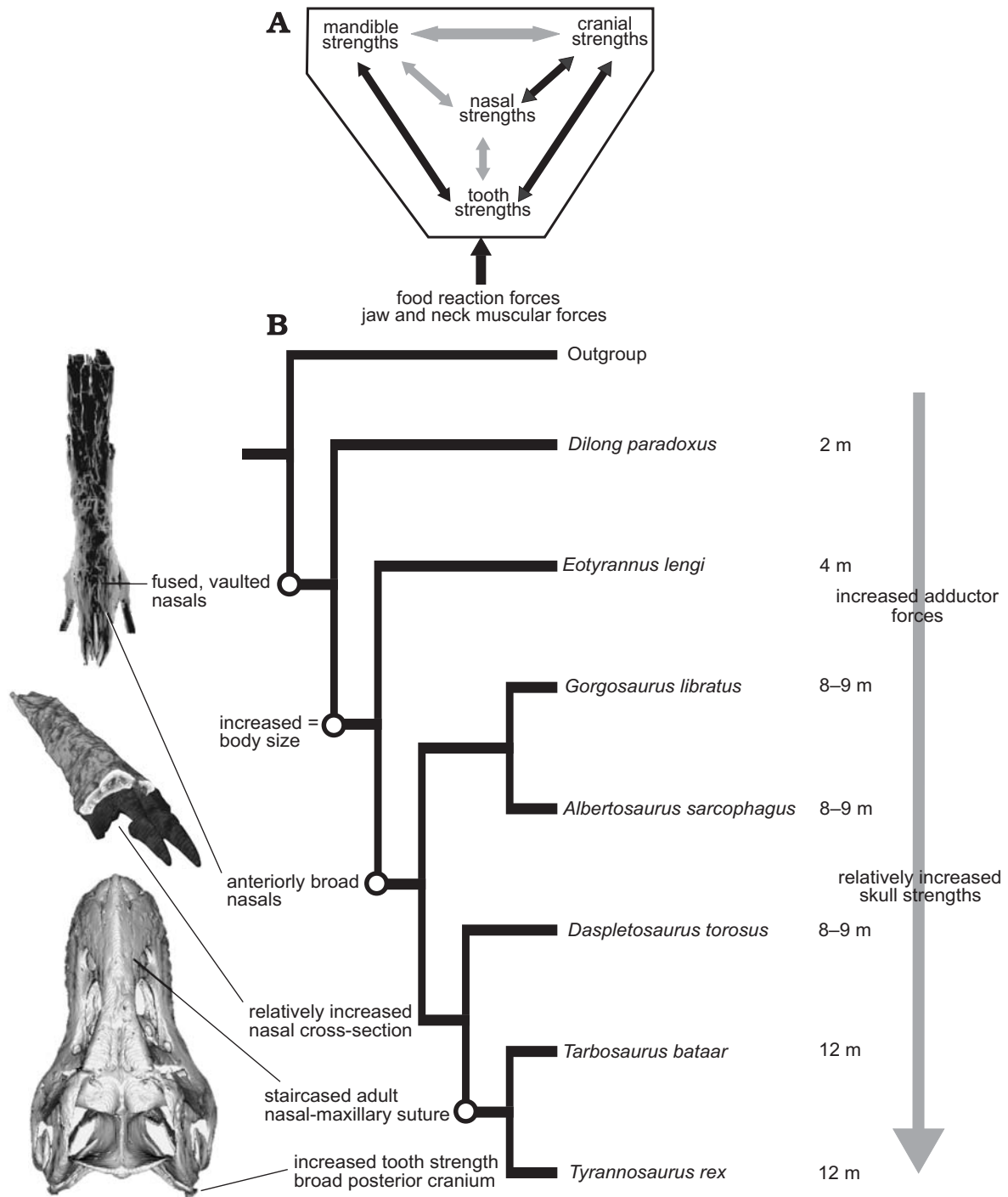


Fig. 14. **A.** Functional integration of strengths of the tyrannosaurid head skeleton when subjected to feeding forces. Dark arrows represent direct influences of forces on structures, and direct integration of structural strengths. Light arrows represent less direct influences of structures on one another. **B.** Correlated progression of tyrannosaurid feeding adaptations mapped onto a tyrannosaurid cladogram after Xu et al. (2004) and Holtz (2004). Arrow at left represents phyletic increases that likely occurred at all ingroup nodes except *G. libratus* + *A. sarcophagus*.

the tyrannosaurids' nasals contributed to overall cranium strength. The breadth of the nasals (Figs. 4 and 10) gave them a high lateral second moment of area, and increased the width of the snout by laterally displacing the maxillae. The great width of the rostrum greatly increased its lateral second moment of area, and overall strength in torsion and lateral bending.

In contrast, the nasals of *Allosaurus* and other carnosaurs are narrow between the articulations with the maxillae (Madsen 1976), the maxillae arch outward less, and the muzzle is consequently narrow (Meers 2003). The narrower rostra of carnosaurs conferred lower lateral bending and torsional strength relative to cranium length than in tyrannosaurids (Fig. 11, Table 2).

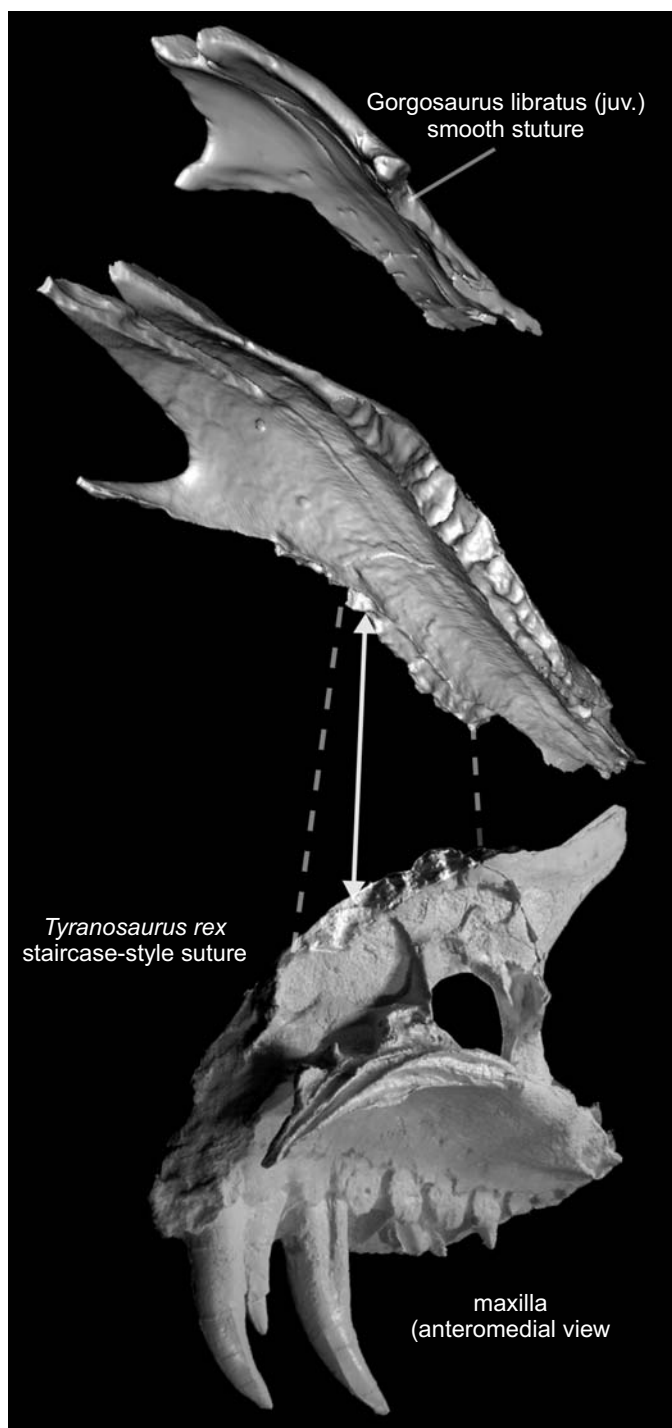


Fig. 15. Nasal articulations with maxillae in juvenile *Gorgosaurus libratus* (nasals at top; TMP 86.144.1) adult *Tyrannosaurus rex* (nasals in middle and maxilla below; TMP 98.86.01; cast of BHI 2033). The interlocking, staircase-style articulation in the adult *Tyrannosaurus rex* efficiently transmitted compressional forces and increased the shear strength of the articulation. Dashed lines show the extent of the staircased articulation, and the solid line indicates a projection on the nasals and the corresponding depression in the maxilla.

High torsional strengths of tyrannosaurid crania and nasals support Holtz's (2002) hypothesis that tyrannosaurids could subject their crania to greater torsional loads than could other

theropods. Combined with strong articulations between bones of the palate, strong nasals and wide muzzles suggest that adult tyrannosaurids engaged in different feeding behaviours than carnosaurs (Holtz 2002).

### Behavioural implications of theropod skull strength

The longer nasal specimens of the tyrannosaurids are stronger than expected than if they were geometrically similar to the nasals of smaller individuals (Fig. 10). The skulls of juvenile tyrannosaurids were proportionally lower than adult skulls (Carr 1999; Currie 2003b), and concomitantly much weaker in vertical bending. Much stronger nasals and allometrically taller skulls in adult tyrannosaurids than in juveniles (Currie 2003b) support hypotheses of dramatic shifts in dietary niche between juveniles and adults (Molnar and Farlow 1990; Holtz 2002).

This ecological partitioning would be similar to that seen in varanid lizards and crocodylians (Bradshaw and Chabreck 1987; Hutton 1987; Losos and Greene 1988), in which the young subsist upon small prey (including insects) and adults tackle much larger animals. Proportionally stronger nasals and crania of adult tyrannosaurids versus juveniles indicate that the adults could probably engage larger prey relative to their own body size.

In the adult cranial specimens examined for this study, the discrepancy in vertical bending strength between tyrannosaurid and carnosaur crania is less than that for lateral strength. With relatively tall, narrow crania, carnosaurs were well equipped to rake down and backwards into the flesh of prey with their upper teeth (Bakker 2000; Rayfield et al. 2001; Antón et al. 2003). Finite element analysis (Rayfield et al. 2001) and consideration of the moment arms of neck muscles (Bakker 2000) demonstrate the probable success of these activities in *Allosaurus fragilis*. High vertical bending strengths of the crania of *Acrocanthosaurus atokensis*, *Carcharodontosaurus saharicus*, and *Sinraptor dongi* suggest the suitability of this strategy for other carnosaurs.

Tyrannosaurid crania were nevertheless relatively stronger dorsoventrally than carnosaur crania, and much stronger in lateral bending and torsion (Holtz 2002). As discussed above, the cranium and nasals would experience high torsional forces from uneven bites, with higher food reaction forces on one side of the skull than the other. Ornithischian fossils damaged during apparently unilateral bites by tyrannosaurids (Erickson and Olson 1996; Wegweiser et al. 2004) indicate that these theropods imposed this loading regime on their crania (Holtz 2002). Adaptations for this biting behaviour would include the great width and height of tyrannosaurid nasals and rostra, a stronger palate than in other theropods (Holtz 2002), and the interdigitating, posteriorly declined mandibular symphysis (Therrien et al. 2005), which increased the torsional strength of the cranium and articulated lower jaws. Additional strength imparted by the staircase-like nasal-maxillary joint of adult *Tarbosaurus bataar* and *Tyrannosaurus rex* would benefit

these 5–10 tonne giants (Paul 1988, Henderson and Snively 2003) when reducing larger prey animals beyond the capacity of other tyrannosaurids.

Potential tyrannosaurid prey (including ceratopsians and hadrosaurs: Russell 1970) were generally smaller than the giant, long-necked sauropods that *Allosaurus* and other carnosaurs more often encountered. It is therefore possible that tyrannosaurids bit into bone more often than would carnosaurs biting into the flesh of larger prey, although fragments in a coprolite (Stone et al. 2000) suggest that large carnosaurs splintered bones before ingestion.

High bending and torsional (Holtz 2002) strength of tyrannosaurid crania and nasals are consistent with biting into bone, but also with adeptness at tearing bone and flesh from large prey (Farlow and Brinkman 1994). High strength in lateral bending suggests the cranium was well equipped to withstand lateral movements of the head and neck while the teeth were embedded in the prey. The great posterior width of tyrannosaurid crania (especially in *Tyrannosaurus rex*) indicates high leverage for muscles that would turn the head (m. longissimus capitis superficialis) or turn and raise it at the same time (m. complexus) during unilateral contraction.

These results complement findings, from tooth marks and finite element analysis, that *Tyrannosaurus rex* was proficient at “puncture and pull” feeding by retraction of the head (Erickson et al. 1996; Rayfield 2004). The high lateral bending strength of tyrannosaurid crania indicates that the animals could have augmented linear retraction with vigorous sideways movements.

High strength of nasals and crania would augment a variety of feeding functions in tyrannosaurids, including the infliction of tissue damage without the need to secure food with their reduced forelimbs (Holtz 2004). Modern carnivorous animals employ forceful bites and lateral tearing of flesh whether killing or eating prey (Auffenberg 1981; Erickson and Olson 1996), and inference of these actions in tyrannosaurids is uninformative for debates over scavenging or predation frequency (Holtz 2002). However, high strength of tyrannosaurid crania indicates that they could afford indelicacy during attempted killing bites (Carpenter 2000; Wegweiser et al. 2004).

## Acknowledgements

This work was supported by an Alberta Ingenuity Studentship and AI research awards to ES, University Technologies Inc. (University of Calgary, Alberta, Canada) awards to DMH, and a Natural Sciences and Engineering Research Council discovery grant to Anthony Russell (University of Calgary). We thank Prathiba Bali (Foothills Hospital radiology department, Calgary, Alberta, Canada) for CT scanning, Heather Jamniczky, Patrick Druckenmiller, David Cooper (all from the University of Calgary), Chris Morrow (Fort Peck Field Station, Montana, USA), Emily Rayfield (Natural History Museum and University of Bristol, UK), and Scott Williams (Burpee Museum, Rockford, Illinois, USA) for discussions, and the staffs at RTMP, UUVF, and BHI. Wendy Sloboda (Warner, Alberta) discovered the *Daspletosaurus* nasals that spurred the project, and Mike Getty (Salt Lake City, Utah, USA) delivered the *Allosaurus* nasals from UUVF.

## References

- Abler, W.L. 1992. The serrated teeth of tyrannosaurid dinosaurs, and biting structures in other animals. *Paleobiology* 18: 161–183.
- Alexander, R.M. 1985. Mechanics of posture and gait of some large dinosaurs. *Zoological Journal of the Linnean Society* 83: 1–25.
- Antón, M., Sánchez I.M., Salesa M.J., and Turner, A. 2003. The muscle-powered bite of *Allosaurus* (Dinosauria; Theropoda): an interpretation of cranio-dental morphology. *Estudios Geológicos* 59: 313–323.
- Auffenberg, W. 1981. *The Behavioral Ecology of the Komodo Monitor*. 406 pp. University of Florida Press, Gainesville.
- Bakker, R.T. 2000. Brontosaur killers: Late Jurassic allosaurids as sabre-toothed cat analogues. *Gaia* 15: 145–158.
- Biewener, A.A. 1992. Overview of structural mechanics. In: A.A. Biewener (ed.), *Biomechanics—Structures and Systems*, 1–20. Oxford University Press, Oxford.
- Bradshaw D.K. and Chabreck R.H. 1987. Alligator feeding habits: new data and a review. *Northeast Gulf Science* 9: 1–8.
- Brochu, C.A. 2003. Osteology of *Tyrannosaurus rex*: insights from a nearly complete skeleton and high-resolution computed tomographic analysis of the cranium. *Journal of Vertebrate Paleontology* 24 (Supplement 4): 1–138.
- Busbey, A.R. 1995. The structural consequences of cranium flattening in crocodylians. In: J.J. Thomason (ed.), *Functional Morphology in Vertebrate Paleontology*, 173–192. Cambridge University Press, Cambridge.
- Carpenter, K. 2000. Evidence of predatory behavior by carnivorous dinosaurs. *Gaia* 15: 136–144.
- Carr, T.D. 1999. Craniofacial ontogeny in Tyrannosauridae (Dinosauria, Coelurosauria). *Journal of Vertebrate Paleontology* 19: 497–520.
- Chin, K., Toyaryk, T.T., Erickson, G.M., and Calk, L.C. 1998. A king-size theropod coprolite. *Nature* 393: 680–682.
- Chure, D.J., Fiorillo, A.R., and Jacobsen, A. 2000. Prey bone utilization by predatory dinosaurs in the Late Jurassic of North America, with comments on prey bone use by dinosaurs throughout the Mesozoic. *Gaia* 15: 227–232.
- Currie, P.J. 2003a. Cranial anatomy of tyrannosaurid dinosaurs from the Late Cretaceous of Alberta, Canada. *Acta Palaeontologica Polonica* 48: 191–226.
- Currie, P.J. 2003b. Allometric growth in tyrannosaurids (Dinosauria: Theropoda) from the Upper Cretaceous of North America. *Canadian Journal of Earth Sciences* 40: 651–665.
- Currie, P.J. and Carpenter K. 2000. A new specimen of *Acrocanthosaurus atokensis* (Theropoda, Dinosauria) from the Lower Cretaceous Antlers Formation (Lower Cretaceous, Aptian) of Oklahoma, USA. *Geodiversitas* 22: 207–246.
- Currie, P.J. and Zhao, X.-J. 1993. A new carnosaur (Dinosauria, Theropoda) from the Jurassic of Xinjiang, People’s Republic of China. *Canadian Journal of Earth Sciences* 30: 2037–2081.
- Erickson, G.M. and Olson, K.H. 1996. Bite marks attributable to *Tyrannosaurus rex*: a preliminary description and implications. *Journal of Vertebrate Paleontology* 16: 175–178.
- Erickson, G.M., Van Kirk, S.D., Su, J., Levenston, M.E., Caler, W.E., and Carter, D.R. 1996. Bite-force estimation for *Tyrannosaurus rex* from tooth-marked bones. *Nature* 382: 706–708.
- Erickson, G. M., Makovicky, P.J., Currie, P.J., Norell, M.A., Yerby, S.A., and Brochu, C.A. 2004. Gigantism and comparative life-history parameters of tyrannosaurid dinosaurs. *Nature* 430: 772–775.
- Farlow, J.O. and Brinkman, D.L. 1994. Wear surfaces on the teeth of tyrannosaurs. In: G.D. Rosenberg and D.L. Wolberg (eds.), *Dino Fest; Proceedings of a Conference for the General Public. Palaeontological Society Special Publications* 7: 165–175.
- Farlow, J.O., Brinkman, D.L., Abler, W.L., and Currie, P.J. 1991. Size, shape, and serration density of theropod dinosaur lateral teeth. *Modern Geology* 16: 161–198.

- Farlow, J.O., Smith, M.B., and Robinson, J.M. 1995. Body mass, bone "strength indicator," and cursorial potential of *Tyrannosaurus rex*. *Journal of Vertebrate Paleontology* 15: 713–725.
- Gordon, J.E. 1978. *Structures: Or Why Things Don't Fall Down*. 395 pp. Plenum Publishing, New York.
- Greaves, W.S. 1978. The jaw lever system in ungulates: a new model. *Journal of Zoology, London* 184: 271–285.
- Greaves, W.S. 1985. The mammalian postorbital bar as a torsion-resisting helical strut. *Journal of Zoology, London* 207: 125–136.
- Greaves, W.S. 1991. The orientation of the force of the jaw muscles and the length of the mandible in mammals. *Zoological Journal of the Linnean Society* 102: 367–374.
- Harris, J.D. 1998. A reanalysis of *Acrocanthosaurus atokensis*, its phylogenetic status, and paleobiogeographic implications, based on a new specimen from Texas. *New Mexico Museum of Nature and Science Bulletin* 13: 1–75.
- Henderson, D. M. 2002. The eyes have it: the sizes, shapes, and orientations of theropod orbits as indicators of cranium strength and bite force. *Journal of Vertebrate Paleontology* 22: 766–778.
- Henderson D.M. and Snively E. 2003. *Tyrannosaurus* en pointe: Allometry minimized rotational inertia of large carnivorous dinosaurs. *Proceedings of the Royal Society B, Biology Letters* 271: S57–S60.
- Holtz, T.R. Jr. 1994. The phylogenetic position of the Tyrannosauridae: implications for theropod systematics. *Journal of Paleontology* 68: 1100–1117.
- Holtz, T.R. Jr. 1995. The arctometatarsalian pes, an unusual structure of Cretaceous Theropoda (Dinosauria: Saurischia). *Journal of Vertebrate Paleontology* 14: 480–519.
- Holtz, T.R. Jr. 2002. Theropod predation: evidence and ecomorphology. In: P.H. Kelly, M. Kowaleski, and T.A. Hansen (eds.), *Predator-Prey Interactions in the Fossil Record. Topics in Geobiology* 17, 325–340. Kluwer/Plenum, New York.
- Holtz, T. R. Jr. 2004. Tyrannosauroida. In: D.B. Weishampel, P. Dodson, and H. Osmólska (eds.), *The Dinosauria*, 111–136. University of California Press, Berkeley.
- Hurum, J.H. and Sabath, K. 2003. Giant theropod dinosaurs from Asia and North America: crania of *Tarbosaurus bataar* and *Tyrannosaurus rex* compared. *Acta Palaeontologica Polonica* 48: 161–190.
- Hutchinson J.R. and Padain K. 1997. Carnosauria. In: P.J. Currie and K. Padian (eds.), *Encyclopedia of Dinosaurs*, 94–97. Academic Press, San Diego.
- Hutt, S., Naish, D.W., Martill, D.M., Barker, M.J., and Newbery, P. 2001. A preliminary account of a new tyrannosaurid theropod from the Wessex Formation (Early Cretaceous) of southern England. *Cretaceous Research* 22: 227–242.
- Hutton, J.M. 1987. Growth and feeding ecology of the Nile crocodile *Crocodylus niloticus* at Ngezi, Zimbabwe. *Journal of Animal Ecology* 56: 25–38.
- Kemp, T.S. 1999. *Fossils & Evolution*. 284 pp. Oxford University Press, Oxford.
- Losos, J.B. and Greene, H.W. 1988. Ecological and evolutionary implications of diet in monitor lizards. *Biological Journal of the Linnean Society* 35: 379–407.
- Madsen, J.H. Jr. 1976. *Allosaurus fragilis*: a revised osteology. *Utah Geological Survey Bulletin* 109: 1–163.
- Mazzetta, G.V., Cislino, A.P., and Blanco, R.E. 2004. Distribución de tensiones durante la mordida en la mandíbula de *Carnotaurus sastrei* Bonaparte, 1985 (Theropoda: Abelisauridae). *Ameghiniana* 41: 605–617.
- Meers, M.B. 2003. Maximum bite force and prey size of *Tyrannosaurus rex* and their relationship to the inference of feeding behaviour. *Historical Biology* 16: 1–12.
- Molnar, R.E. 1973. *The Cranial Morphology and Mechanics of Tyrannosaurus rex (Reptilia: Saurischia)*. 447 pp. PhD thesis, University of California, Los Angeles.
- Molnar, R.E. 2000. Mechanical factors in the design of the cranium of *Tyrannosaurus rex* (Osborn 1905). *Gaia* 15: 193–218.
- Molnar, R.E. and Farlow J.O. 1990. Carnosaur paleobiology. In: D.B. Weishampel, P. Dodson, and H. Osmólska (eds.), *The Dinosauria*, 221–224. University of California Press, Berkeley.
- Paul, G.S. 1988. *Predatory Dinosaurs of the World*. 464 pp. Simon and Schuster, New York.
- Rayfield, E.J. 2004. Cranial mechanics and feeding in *Tyrannosaurus rex*. *Proceedings of the Royal Society of London B* 271: 1451–1459.
- Rayfield, E. J. 2005. Using finite element analysis to investigate suture morphology: a case study using large carnivorous dinosaurs. *The Anatomical Record Part A* 283A: 349–365.
- Rayfield, E.J., Norman, D.B., Horner, C.C., Horner, J.R., May Smith, P., Thomason, J.J., and Upchurch, P. 2001. Cranial design and function in a large theropod dinosaur. *Nature* 409: 1033–1037.
- Russell, D.A. 1970. Tyrannosaurs of the Late Cretaceous of western Canada. *National Museum of Natural Sciences, Publications in Palaeontology* 1: 1–34.
- Sereno, P.C., Dutheil, D.B., Iarochene, M., Larsson, H.C.E., Lyon, G.H., Magwene, P.M., Sidor, C.A., Varricchio, D.J., and Wilson, J.A. 1996. Predatory dinosaurs from the Sahara and late cretaceous faunal differentiation. *Science* 272: 986–991.
- Slijper, E.J. 1946. Comparative biologic-anatomical investigations on the vertebral column and spinal musculature of mammals. *Verhandelingen der Koninklijke Nederlandse Akademie van Wetenschappen, Afdeling Natuurkunde (Tweede Sectie)* 42: 1–128.
- Snively, E. and Russell, A.P. 2002. The tyrannosaurid metatarsus: bone strain and inferred ligament function. *Senckenbergiana lethaea* 82: 35–42.
- Snively, E. and Russell, A.P. 2003. A kinematic model of tyrannosaurid (Dinosauria, Theropoda) arctometatarsus function. *Journal of Morphology* 255: 215–227.
- Snively, E., Russell, A.P., and Powell, G.L. 2004. Evolutionary morphology of the coelurosaurian arctometatarsus: descriptive, morphometric, and phylogenetic approaches. *Zoological Journal of the Linnean Society* 142: 525–553.
- Stone, D.W., Crisp, E.L., and Bishop J.R. 2000. A large meat-eating dinosaur coprolite from the Jurassic Morrison Formation of Utah. *Geological Society of America Annual Meeting. Abstracts with Programs* 32: 220.
- Therrien, F., Henderson, D.M., and Ruff, C.B. 2005. Bite me: biomechanical models of theropod mandibles and implications for feeding behavior. In: K. Carpenter (ed.), *The Carnivorous Dinosaurs*, 179–237. Indiana University Press, Bloomington.
- Thomason, J.J. and Russell, A.P. 1986. Mechanical factors in the evolution of the mammalian secondary palate. *Journal of Morphology* 189: 199–213.
- Thompson, D.A. 1917. *On Growth and Form* (edited by Bonner, J.T.). 368 pp. Cambridge University Press, Cambridge (1992 edition).
- Thomson, K.S. 1966. The evolution of the tetrapod middle ear in the rhipidistian-tetrapod transition. *American Zoologist* 6: 379–397.
- Wegweiser, M., Breithaupt, B., and Chapman, R. 2004. Attack behavior of tyrannosaurid dinosaur(s): Cretaceous crime scenes, really old evidence, and "smoking guns". *Journal of Vertebrate Paleontology* 24 (Supplement 3): 127A.
- Witmer, L.M. 1997. The evolution of the antorbital cavity of archosaurs: a study in soft-tissue reconstruction in the fossil record with an analysis of the function of pneumaticity. *Journal of Vertebrate Paleontology* 17 (Supplement 1): 1–73.
- Xu, X., Clark, J.M., Forster C.A., Norell M.A., Erickson, G.M., Eberth, D.A., Jia, C., and Zhao, Q. 2006. A basal tyrannosauroid dinosaur from the Late Jurassic of China. *Nature* 439: 715–718.
- Xu X., Norell, M.A., Kuang, X., Wang, X., Zhao, Q., and Jia, C. 2004. Basal tyrannosauroids from China and evidence for protofeathers in tyrannosauroids. *Nature* 431: 680–684.
- Young, W.C. and Budynas, R. 2001. *Roark's Formulas for Stress and Strain*. 832 pp. McGraw-Hill, New York.

## Appendix 1

Theropod specimens used for tooth, nasal, and cranial strength calculations. Symbols used in diagrams are given in parentheses for each specimen, followed by its specimen number and/or literature source.

Maxillary teeth: Fig. 3	Tyrannosauridae	<i>Albertosaurus sarcophagus</i> (As) <i>Daspletosaurus torosus</i> (DtL) <i>Daspletosaurus</i> sp. juv. (DtS) <i>Gorgosaurus libratus</i> (Gl) <i>Gorgosaurus libratus</i> (GIL) <i>Tyrannosaurus rex</i> (TrA) <i>Tyrannosaurus rex</i> (TrB) <i>Tyrannosaurus rex</i> (TrL) <i>Tyrannosaurus rex</i> juv. (TrJ)	TMP 81.10.1 TMP 2001.36.1 TMP 1994.143.1 ROM 1247 TCMI 2001.89.01 (TMP 2004.03.04) AMNH 5027 BHI 2033 (TMP 98.86.1) LACM 7244/2384 BMRP 2002.4.1 (TMP 2004.03.03)
	Carnosauria	<i>Acrocanthosaurus atokensis</i> (Aa) <i>Allosaurus fragilis</i> (Af) <i>Monolophosaurus jiangi</i> (Mj) <i>Sinraptor dongi</i> (Sd)	Harris 1998; Currie and Carpenter 2000 ROM 5091 IVPP 84019 IVPP 10600
	Neoceratosauria	<i>Carnotaurus sastrei</i> (Cs) <i>Ceratosaurus dentisulcatus</i> (Cd)	MACN-CH 894 MWC 0001
Nasals: Fig. 8	Tyrannosauridae	<i>Albertosaurus sarcophagus</i> (As) <i>Daspletosaurus torosus</i> (Dt) <i>Gorgosaurus libratus</i> (Gl) juvenile <i>Gorgosaurus libratus</i> (Gl) <i>Tyrannosaurus rex</i> (Tr)	TMP 2000.12.1 TMP 98.48.1 TMP 86.144.1 TMP 96.64.1 BHI 2033
	Carnosauria	<i>Allosaurus fragilis</i> (Af) juvenile <i>Allosaurus fragilis</i> (Af) medium <i>Allosaurus fragilis</i> (Af) large	UUVP 10854/UMNH VP 7784 UUVP 1913/UMNH VP 9144 UUVP 1663/UMNH VP 9146
Crania: Figs. 11, 13	Tyrannosauridae	<i>Daspletosaurus torosus</i> (Dt) <i>Gorgosaurus libratus</i> (Gl) <i>Tyrannosaurus rex</i> (TrA) <i>Tyrannosaurus rex</i> (TrF)	NMC 8505; Russell 1970 ROM 1247; Carr 1999 AMNH 5027; Paul 1988 FMNH PR2081; Brochu 2003
	Carnosauria	<i>Acrocanthosaurus atokensis</i> (Aa) <i>Allosaurus fragilis</i> (Af) <i>Carcharodontosaurus saharicus</i> (Cs) <i>Sinraptor dongi</i> (Sd)	NCSM 14345; Currie and Carpenter 2000 MOR 693; Rayfield et al. 2001 SGM-Din1; Sereno et al. 1996 IVPP 10600; Currie and Zhao 1993

## Appendix 2

Determination of the centroid of a sub-triangle of a nasal cross-section

The region bounded by a contour outlining a nasal bone cross-section was decomposed into sub-triangles using the method of Henderson (2002). For the  $i^{\text{th}}$  sub-triangle, its centroid ( $z_i, y_i$ ) was computed as the point of intersection of two lines that originate at two vertices and intersect the midpoints of their respective opposite sides of the triangle. The slope,  $m_A$ , and intercept,  $b_A$ , of one of these lines originating from a vertex A, ( $line_A$ ), are determined from:

$$m_A = \frac{MP_{BC}^y - y_A}{MP_{BC}^z - z_A} \quad (A1)$$

$$b_A = y_A - m_A \cdot z_A \quad (A2)$$

where  $MP_{BC}$  is the midpoint of the edge  $\overline{BC}$  and is expressed as:

$$MP_{BC} = \frac{1}{2} \cdot \left( \begin{bmatrix} z \\ y \end{bmatrix}_B + \begin{bmatrix} z \\ y \end{bmatrix}_C \right) \quad (A3)$$

With similar expressions for the slope and intercept of a line originating from a third vertex ( $line_C$ ), the horizontal coordinate of the point of intersection of lines A and C comes from equating lines A and C, and solving for  $z_i$ :

$$z_i = \frac{b_C - b_A}{m_A - m_C} \quad (A4)$$

With the slope and intercept of  $line_C$  the vertical coordinate of intersection is:

$$y_i = b_C + m_C \cdot z_i \quad (A5)$$